Variational methods for tomographic reconstruction with few views

Maïtine Bergounioux, Isabelle Abraham, Romain Abraham, Guillaume Carlier, Erwan Le Pennec, Emmanuel Trélat

Variational methods for tomographic reconstruction with few views

Maïtine Bergounioux, Isabelle Abraham, Romain Abraham, Guillaume Carlier, Erwan Le Pennec and Emmanuel Trélat

Abstract. We deal with a severe ill posed problem, namely the reconstruction process of an image during tomography acquisition with (very) few views. We present different methods that we have been investigated during the past decade. They are based on variational analysis. This is a survey paper and we refer to the quoted papers for more details.

Mathematics Subject Classification (2010). 49K40, 45Q05,65M32.

Keywords. tomographic reconstruction, variational method, optimal transport, Radon operator, inverse problem, fractional order Hilbert spaces, needlets.

1. Introduction

This survey paper is devoted to a specific application of tomographic reconstruction for a physical experiment whose goal is to study the behavior of a material under a shock. We describe the motivating experiment in the sequel. This leads to severely ill posed inverse problems. Indeed, the classical tomography reconstruction process (involving the Radon operator that we depict in Section 2.1) is well posed in the case where there is an infinite number of data. In most cases (medical imaging for example) there are a lot of data (though the number is of course finite) and the classical filtered back projection method (that use the Fourier slice theorem) provides good results and overcome the lack of well posedness. However, there are many situations when there is *not enough* data: this happens for limited view angles (see [33] for example) or when it is impossible to get more than two or three views. This is the case of the experiment, depicted on Figure 1.1, that consists in causing the implosion of the hull of some material (usually, a metal) whose features are well known, using surrounding explosives. The problem is to determine the shape of the interior interface at a specific moment of the implosion. For

this purpose, a single X-ray radiography is performed, and the shape of the object must then be reconstructed using a tomographic approach.

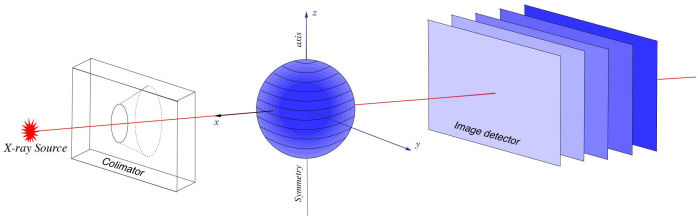

FIGURE 1.1. Experimental setup.

As mentioned before, when enough projections of the object, taken from different angles, are available, several techniques exist for tomographic reconstruction, providing an analytic formula for the solution (see for instance [30] or [23]). There is a huge literature about theoretical and practical aspects of the problem of reconstruction from projections, the applications of which concern medicine, optics, material science, astronomy, geophysics, and magnetic resonance imaging (see [10]). An important application is the problem of medical transmission X-ray tomography (see [32]), in which X-rays are fired from many angles through a single cross section of the body, measuring line integrals of the linear attenuation coefficient of the object. The resulting collection of projections then permits to reconstruct the 3D body.

When only few projections are known, these methods cannot be used directly, and some alternative methods have been proposed to reconstruct partially the densities (see for instance [22]) As in any tomographic reconstruction process, this problem leads to an ill-posed inverse problem. Since we only have few radiographs at our disposal, data are not redundant and the ill-posed character is even more accurate. Moreover, the flash has to be very brief (several nanoseconds) due to the imploding movement of the hull. Such X-rays cannot be provided by standard sources, and hence numerous drawbacks appear, for instance the X-rays beam is not well focused and the X-rays source is not punctual. This causes a blur on the radiograph. Furthermore, contrarily to medical radiography where photons are absorbed by bones, here X-rays must cross a very dense object and therefore must be of high energy. Most of the photons are actually absorbed by the object and only a few number of them arrive at the detector. It is therefore necessary to add some amplification devices and very sensitive detectors, which cause a high noise level and another blur.

In this paper, we give an overview of the techniques that have been developed during the past decade by the authors of the present paper [3, 4, 15] and other collaborators. It would be too long to report on every technique we investigated but one can refer to [1, 2, 13, 14] as well. Let us point out that we decided to use variational methods because they are a quite efficient tool to deal with inverse problems. As most of the results have been published

we do not give proofs and refer to the corresponding papers. However, we have to mention that Section 4 is new and remained unpublished until now. Therefore we give more details.

The paper is organized as follows. We first assume that the object to reconstruct is **radially symmetric**; we present in Section 2 the problem and the mathematical framework (operators and mathematical tools). Section 3 deals with the case where there is only one projection (and the object to recover is still assumed to be axially symmetric). We present theoretical results there while Section 4 is devoted to numerical realization (both algorithms and results). In Section 5 **we abandon the axisymmetry** assumption and investigate a different modeling via optimal transport techniques.

2. Setting the problem

2.1. The operators

Radiography measures the attenuation of X-rays through the object. Recall that we consider a radially symmetric object. A point on the radiograph is determined by Cartesian coordinates (y, z), where the z axis is the symmetry axis. Let I_0 denote the intensity of the incident X-rays flux. Then, the measured flux $I(y, z)$ at a point (y, z) is given by

$$I = I_0 e^{-\int \mu(r,z) d\ell},$$

where the integral operates along the ray that reaches the point (y, z) of the detector, $d\ell$ is the infinitesimal element of length along the ray, and μ is the linear attenuation coefficient. Considering the Neperian logarithm of this attenuation permits to deal rather with linear operators, and the linear mapping

$$\mu \longmapsto \int \mu d\ell$$

is called the *projection operator*.

In practice, the ratio of the diameter of the object by the distance "X-ray source - object" is small, and we assume for the sake of simplicity, that the rays are parallel, and orthogonal to the symmetry axis. It follows that horizontal slices of the object can be considered separately to perform the projection. In these conditions, for a 3D object represented by a linear attenuation coefficient $\tilde{u}(x, y, z)$ (with compact support) in Cartesian coordinates, the projection operator H_0 can be written

$$(H_0\tilde{u})(y, z) = \int_{\mathbb{R}} \tilde{u}(x, y, z) dx. \tag{2.1}$$

Since we assume that the objects are bounded and axially symmetric, it is relevant to make use of cylindrical coordinates (r, θ, z), where the z-axis designates the symmetry axis. Such objects are represented by a linear attenuation coefficient $u(r, z)$, where u denotes a function of $L^\infty(\mathbb{R}_+ \times \mathbb{R})$ with compact support. In the sequel, all such functions are assumed to have a compact support contained in the subset $\Omega = [0, a) \times (-a, a)$ of $\mathbb{R}^2$, where $a > 0$ is

fixed. Then, one defines $H_0u = H_0\tilde{u}$, where $\tilde{u}(x,y,z) = u(\sqrt{x^2+y^2}, z)$ for all $x, y, z \in \mathbb{R}$, and where $H_0\tilde{u}$ is defined by (2.1). An obvious change of variable leads to

$$(H_0u)(y,z) = 2\int_{|y|}^{+\infty} u(r,z)\,\frac{r}{\sqrt{r^2-y^2}}dr, \tag{2.2}$$

for almost all $y, z \in \mathbb{R}$.

It is clear that the function H_0u is of compact support contained in $\tilde{\Omega} = (-a,a)^2$. In what follows, functions of compact support contained in Ω (resp., in $\tilde{\Omega}$) and their restriction to Ω (resp., in $\tilde{\Omega}$) are denoted similarly. Moreover H_0 extends to a linear operator (still denoted H_0) on $L^p(\Omega)$, for every $p \in [1,+\infty]$. In particular, $H_0 : L^p(\Omega) \to L^s(\tilde{\Omega})$ is a continuous linear operator, for every $p \in [1,+\infty]$ and every s such that $s \in [p, \frac{2p}{2-p})$ whenever $1 \le p \le 2$, and $s \in [p,+\infty]$ whenever $p > 2$. In particular, $H_0 : L^2(\Omega) \to L^2(\tilde{\Omega})$ is a continuous linear operator. Let $H_0^* : L^2(\tilde{\Omega}) \to L^2(\Omega)$ denote the adjoint operator of H_0 (i.e., the back-projection operator), for the pivot space L^2, i.e., $\langle H_0u, v\rangle_{L^2(\tilde{\Omega})} = \langle u, H_0^*v\rangle_{L^2(\Omega)}$, for every $u \in L^2(\Omega)$ and every $v \in L^2(\tilde{\Omega})$. An obvious computation gives

$$(H_0^*v)(r,z) = 2\int_{-r}^{r} v(y,z)\frac{r}{\sqrt{r^2-y^2}}dy, \tag{2.3}$$

for every $(r,z) \in \Omega$. Similarly, the operator H_0^* extends to a continuous linear operator $H_0^* : L^{s'}(\tilde{\Omega}) \to L^{p'}(\Omega)$, for every $s' \in [1,+\infty]$ and every p' such that $p' \in [s', \frac{2s'}{2-s'})$ whenever $1 \le s' \le 2$, and $p' \in [s',+\infty]$ whenever $s' > 2$.

The operator H_0 features the Radon transform of the object. For more details on the Radon transform , see [8, 26, 27, 28, 36] for example. Practically, one radiograph suffices to reconstruct the object. From the theoretical point of view, inverting the operator H_0 requires further differentiability. More precisely, the next lemma holds.

Lemma 2.1. *Let $g \in L^2(\tilde{\Omega})$ such that $g(y,z) = g(-y,z)$ for a.e. $(y,z) \in \tilde{\Omega}$ and such that $\frac{\partial g}{\partial y}$ exists almost everywhere on $\tilde{\Omega}$ and is measurable and bounded. Then, there exists a unique $u \in L^\infty(\Omega)$ such that $H_0u = g$, and*

$$u(r,z) = -\frac{1}{\pi}\int_r^a \frac{\partial g}{\partial y}(y,z)\frac{1}{\sqrt{y^2-r^2}}dy,$$

for every $(r,z) \in \Omega$.

Without any ambiguity, we denote $u = H_0^{-1}g$, and this defines the linear operator H_0^{-1} that can be extended to a continuous linear operator $H_0^{-1} : W^{1,p}(\tilde{\Omega}) \to L^s(\Omega)$, for every $p \in [1,+\infty]$ and every s such that $s \in [p, \frac{2p}{2-p})$ whenever $1 \le p \le 2$, and $s \in [p,+\infty]$ whenever $p > 2$. However, because of the derivative term, the operator H_0^{-1} cannot be extended as a continuous linear operator from $L^p(\Omega)$ to $L^q(\Omega)$ for suitable p and q. Concretely, this means that a small variation of the measure induces significant errors on the reconstruction. Since the radiographs at our disposal are

strongly perturbed, applying H_0^{-1} thus provides a deficient and imperfect reconstruction of the original image. Moreover, due to the experimental setup, there are two additional main perturbations:

- A *blur*, due to the detector response and the X-ray source spot size. To simplify, it is assumed that the effect B of the blur is linear, and writes
$$Bu_d = K \star u_d, \tag{2.4}$$
where $\star$ is the usual convolution operation, u_d is the projected image, and K is a positive symmetric kernel with compact support and such that $\int K d\mu = 1$.
- A *noise*, assumed to be an additive Gaussian white noise, denoted τ, of zero mean and of standard deviation σ_τ.

Others perturbations, such as scattered field or motion blur, are not taken into account in our study. With these assumptions, the projection of an object u is
$$v_d = BH_0u + \tau.$$

A useful tool to deal with ill-posed problems is a regularization process based on optimization methods. This is what we describe in the sequel.

2.2. Mathematical tools

The most suitable functional space used in image restoration is the space $\mathrm{BV}(\Omega)$ of bounded variation functions defined by
$$\mathrm{BV}(\Omega) = \{u \in L^1(\Omega) \mid TV(u) < +\infty\},$$
where
$$TV(u) = \sup\left\{\int_\Omega u(x) \operatorname{div} \xi(x)\, dx \mid \xi \in \mathcal{C}_c^1(\Omega),\ \|\xi\|_\infty \le 1\right\}. \tag{2.5}$$
The space $\mathrm{BV}(\Omega)$, endowed with the norm $\|u\|_{\mathrm{BV}(\Omega)} = \|u\|_{L^1} + TV(u)$, is a Banach space. The derivative in the sense of the distributions of every $u \in \mathrm{BV}(\Omega)$ is a bounded Radon measure, denoted Du, and $TV(u) = \int_\Omega |Du|$ is the total variation of Du. Standard properties of bounded variation functions can be found in [6, 9].
We will also need a definition of fractional order Hilbert spaces. Let U be an open subset of $\mathbb{R}^n$. For $k \in \mathbb{N}$, the Hilbert space $H^k(U)$ is defined as the space of all functions of $L^2(U)$, whose partial derivatives up to order k, in the sense of distributions, can be identified with functions of $L^2(U)$. Endowed with the norm
$$\|f\|_{H^k(U)} = \left(\sum_{|\beta|\le k} \|D^\beta f\|^2_{L^p(U)}\right)^{1/2},$$
$H^k(U)$ is a Hilbert space. For $k = 0$, there holds $H^0(U) = L^2(U)$. Here $\beta = (\beta_1, \cdots, \beta_n)$ is a multi-index such that $|\beta| = \sum_{i=1}^n \beta_i \le k$ and $D^\beta f := \partial_{x_1}^{\beta_1} f \cdots \partial_{x_n}^{\beta_n} f$.

For $s \in (0,1)$, the fractional order Hilbert space $H^s(U)$ is defined as the space of all functions $f \in L^2(U)$ such that (see [18])

$$\iint_{U\times U} \frac{|f(x)-f(y)|^2}{|x-y|^{n+2s}} dx\, dy \ < +\infty.$$

Endowed with the norm

$$\|f\|_{H^s(U)} = \left(\|f\|^2_{L^2(U)} + \iint_{U\times U} \frac{|f(x)-f(y)|^2}{|x-y|^{n+2s}} dx\, dy \right)^{1/2},$$

$H^s(U)$ is a Hilbert space.

3. Variational models for axially symmetric objects

To simplify the problem we first assume that all components of the initial physical setup are axially symmetric and remain as such during the implosion process. Therefore a single radiograph of the cross section suffices in theory to reconstruct the 3D object. As X-rays are assumed to be parallel, "horizontal" slices of the object are independent and are treated separately. Hence, usual regularization techniques for tomography (such as filtered backprojection) are not adapted, since they deal with one particular slice. Here, because of the axial symmetry, slices are composed of concentric annuli and do not need any regularization. On the contrary, some regularity between the different slices is required, and only few results in that direction are known (see [17, 22]).

Another difficulty is that we deal with *binary objects* composed of one homogeneous material (drawn in black) and of some holes (in white). Our working example, drawn on Figure 3.1, represents a synthetic object containing all standard difficulties that may appear, such as:

- several disconnected holes;
- a small hole located on the symmetry axis (where details are expected to be difficult to recover because the noise variance is maximal around the symmetry axis after reconstruction);
- smaller details on the boundary of the top hole, serving as a test for lower bound detection.

Figure 3.1(a) shapes an object composed of concentric shells of homogeneous materials surrounding a ball (called the "interior") of another homogeneous material containing empty holes. It can be viewed as the slice of a axially symmetric 3D object by a plane containing the symmetry axis of that object. A rotation of the image of Figure 3.1(a) around the z axis must be performed in order to recover the 3D-object, in which, for instance, the two white holes generate a torus. Since the object is mainly featured in the shape of the holes, in the sequel we will focus on the interior of the object (see Figure 3.1(b)).

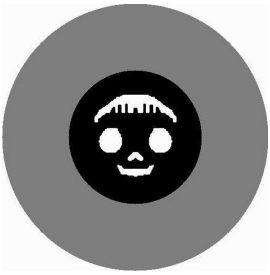

(a) Slice of an axially symmetric object by a plane containing the symmetry axis.

(b) Zoom on the interior of the object of Figure 3.1(a); the homogeneous material is drawn in black and the holes in white.

FIGURE 3.1. Working example.

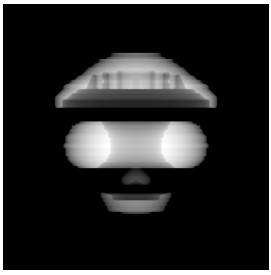

(a) Theoretical projection H_0u of the object of Figure 3.1.

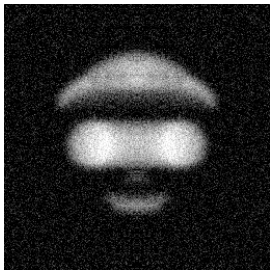

(b) Real projection $v_d = BH_0u + \tau$ of the same object with realistic noise and blur.

(c) The real object u.

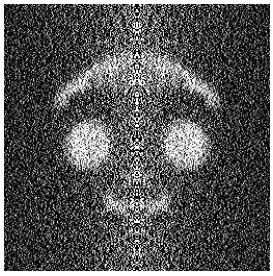

(d) Reconstruction $H_0^{-1}v_d$ computed with H_0^{-1} applied to the real projection.

FIGURE 3.2. Comparison of u, BH_0u, $v_d = BH_0u + \tau$, $H_0^{-1}v_d$.

Based on a single X-ray radiograph which is at our disposal, it is our aim to perform a tomographic reconstruction to reconstruct the whole axially symmetric object. We review in this paper different variational methods adapted to the tomographic reconstruction of blurred and noised binary images, based on a minimization problem. Note that our approach is global, contrarily to usual methods of reconstruction rather dealing with a line-by-line analysis carried out on each line of the radiograph (see [29]). A comparison between the theoretical projection H_0u and the perturbed one is provided on Figures 3.2(a) and 3.2(b). The real object u is drawn on Figure 3.2(c). The reconstruction using the inverse operator H_0^{-1} applied to v_d is drawn on Figure 3.2(d). The purpose of the experiment is to separate the material from the empty holes and thus to determine precisely the boundary between the two areas. This task is difficult to perform on the reconstruction $H_0^{-1}v_d$, and an inspection of Figure 3.2(d) shows that the use of the inverse operator is not suitable.

3.1. A first variational model

We first proposed in [4] a variational method based on a minimization problem in the space of bounded variation functions, proved existence and uniqueness results. The binary structure of the material under consideration is modeled as a binary constraint: the intensity function is either equal to 0 or 255 (normalized to 0 and 1). Due to this binary constraint, deriving an optimality system is not straightforward, and we proposed a penalization method for which we established some properties and derived an optimality system. Assume that the kernel K modeling the blur has a compact support contained in $\tilde{\Omega}$. Then, the operator B defined by (2.4) is a continuous linear operator from $L^p(\tilde{\Omega})$ to $L^q(2\tilde{\Omega})$, for all $p, q \in [1, +\infty]$, where $2\tilde{\Omega} = (-2a, 2a)^2$.

Let $v_d \in L^2(\tilde{\Omega})$ be the projected image (observed data), and let $\alpha > 0$. Define $H = BH_0$, and consider the minimization problem

$$(\mathcal{P}) \qquad \begin{cases} \min F(u), \quad \text{with } F(u) = \dfrac{1}{2}\|Hu - v_d\|_2^2 + \alpha TV(u), \\ u \in \mathrm{BV}(\Omega), \\ u(x) \in \{0, 1\} \text{ a.e. on } \Omega, \end{cases}$$

where $\|\cdot\|_2$ stands for the $L^2(\tilde{\Omega})$ norm.

Theorem 3.1. *The minimization problem $(\mathcal{P})$ admits at least a solution.*

To deal with the binary constraint set whose interior in suitable topologies may be empty, we use a penalization method that allows to relax this constraint. Precisely, let $\varepsilon > 0$, $\beta \geq 0$, and let $\bar{u}$ be a solution to $(\mathcal{P})$. Define

$$F_\varepsilon(u) = F(u) + \frac{1}{2\varepsilon}\|u - u^2\|_2^2 + \frac{\beta}{2}\|u - \bar{u}\|_2^2.$$

We consider the penalized problem

$$(\mathcal{P}_\varepsilon) \qquad \begin{cases} \min F_\varepsilon(u) \\ u \in \mathrm{BV}(\Omega) \cap \mathcal{B}_R \end{cases}$$

where $R > 1$ is a fixed real number, and

$$\mathcal{B}_R = \{u \in L^\infty(\Omega) \mid \|u\|_\infty \leq R\}.$$

In the sequel we do not mention the dependence of $(\mathcal{P}_\varepsilon)$ with respect to the real number R that can be chosen as large as desired but is fixed. A contrario the parameter ε will tend to 0. Note that the constraint $u \in \mathcal{B}_R$ is required theoretically to ensure convergence properties, however it does not affect the numerical process. Then we get approximation results:

Theorem 3.2. 1. *The minimization problem* $(\mathcal{P}_\varepsilon)$ *has at least a solution* $u_\varepsilon \in \mathrm{BV}(\Omega) \cap \mathcal{B}_R$.

2. *Every cluster point* u^* *in* $\mathrm{BV}(\Omega) \cap L^p(\Omega)$ *(for* $p \in [1, +\infty)$*) of the family* (u_ε) *at* $\varepsilon = 0$ *is a solution of* $(\mathcal{P})$. *If moreover* $\beta > 0$ *then* $u^* = \bar{u}$.

3. *There holds* $\lim_{\varepsilon \to 0} F_\varepsilon(u_\varepsilon) = \inf F$, *and* $\lim_{\varepsilon \to 0} \int_\Omega |Du_\varepsilon| = \int_\Omega |Du|$.

Then using [20, Theorem 2.3] we get

Theorem 3.3. *Let* u_ε *be a solution of* $(\mathcal{P}_\varepsilon)$. *Then there exist* $\lambda_\varepsilon \in (\mathcal{M}(\Omega)^2)'$, $q_\varepsilon \in L^\infty(\Omega)$ *and* $\mu_\varepsilon = -div\ \lambda_\varepsilon$ *such that*

$$\forall u \in \mathrm{BV}(\Omega) \cap \mathcal{B}_R \qquad \langle H^*(Hu_\varepsilon - v_d) + q_\varepsilon + \alpha\mu_\varepsilon, u - u_\varepsilon \rangle \geq 0\ , \tag{3.1a}$$

$$\mu_\varepsilon \in \partial TV(u_\varepsilon)\ , \tag{3.1b}$$

Here $\mathcal{M}(\Omega)$ stands for the space of Radon measures on Ω. In order to derive an optimality system for the minimization problem $(\mathcal{P})$, it would be natural to attempt to pass to the limit in (3.1a)-(3.1b). However, this not possible since we cannot obtain estimates that would allow to do it. This is certainly due to the fact that the set of binary constraints has an empty L^∞ interior. As a consequence, we cannot bound the family (q_ε) uniformly (in $H^{-1}(\Omega)$) with respect to ε. Nevertheless, though it would be theoretically satisfying to get such a limit optimality system, it is not directly useful from the numerical point of view and we use the penalized one.

3.2. Improving the model with fractional framework

In [15] we made a refined study of the intrinsic regularity properties of the projection operator, which leads to reconsider the above minimization procedure with a more adapted norm.Then, combining this theoretical study with a careful numerical implementation leads to spectacular numerical improvements.

3.2.1. Refined functional properties of the Radon operator. Regularity properties of the Radon transform and their applications to tomography have been widely investigated in the literature (see e.g. [4, 25, 26, 27, 28, 36]), but are generally stated in the spaces L^p. As mentioned above, it has been shown in [4] that the use of such norms indeed provides acceptable reconstruction processes, but they will happen to be largely improved by taking into account stronger regularity features. A refined functional analysis of the Radon projection operator H_0 defined by (2.2) was led in [15], stating that it enjoys

strong regularity properties in fractional order Hilbert spaces. We next recall these results. Denote by

$$X = L^2(-a,a;BV_0(0,a)) \tag{3.2}$$

the set of all functions $u \in L^2(\Omega)$ such that the function $(z,r) \mapsto u(r,z)$ belongs to $L^2(-a,a;BV_0(0,a))$, where $BV_0(0,a)$ is the closed subset of the set of functions $f \in BV(0,a)$ vanishing at a. The total variation, which is a semi-norm, is a norm on $BV_0(0,a)$. Hence the space X is a closed subspace of the Banach space $L^2(-a,a;BV(0,a))$, and can be endowed with the norm

$$\|u\|_X = \left(\int_{-a}^{a} (|Du_z|(0,a))^2\, dz\right)^{1/2} = \left(\int_{-a}^{a} (TV_1(u_z))^2\, dz\right)^{1/2}, \tag{3.3}$$

where the notation u_z stands for the function $r \mapsto u_z(r) = u(r,z)$, and where the notation $TV_1(f)$ is used to denote the total variation of a function $f \in BV(0,a)$ while $TV(f)$ denotes the total variation of a function of $\mathrm{BV}(\Omega)$.

For every $s \in (0,1)$, the fractional order Hilbert space $H^s(-a,a)$ is defined as the space of all functions $f \in L^2(-a,a)$ such that

$$\int_{-a}^{a}\int_{-a}^{a} \frac{|f(x)-f(y)|^2}{|x-y|^{1+2s}} dx\, dy \ < +\infty,$$

endowed with the norm

$$\|f\|_{H^s(-a,a)} = \left(\|f\|^2_{L^2(-a,a)} + \int_{-a}^{a}\int_{-a}^{a} \frac{|f(x)-f(y)|^2}{|x-y|^{1+2s}} dx\, dy\right)^{1/2}.$$

It is possible to define the Hilbert space $H^s(-a,a)$ in other equivalent ways, in particular with the Fourier transform or with the fractional Laplacian operator (see [15] for a survey of equivalent definitions).

The space $H^s_0(-a,a)$ is defined as the closure in $H^s(-a,a)$ of the set of all smooth functions having a compact support contained in $(-a,a)$. Note that, for $s \in [0,1/2]$, there holds $H^s_0(-a,a) = H^s(-a,a)$. The Lions-Magenes space $H^{1/2}_{00}(-a,a)$ is the subset of functions $f \in H^{1/2}(-a,a)$ such that $\rho^{-1/2} f \in L^2(-a,a)$, where the function ρ is defined on $(-a,a)$ by $\rho(y) = a - |y|$.

For every $s \in [0,1) \setminus \{1/2\}$, denote by

$$Y_s = L^2(-a,a;H^s_0(-a,a)) \tag{3.4}$$

the set of all functions $v \in L^2(\Omega_1)$ such that the function $(z,y) \mapsto v(y,z)$ belongs to $L^2(-a,a;H^s_0(-a,a))$. It is a closed subspace of $L^2(-a,a;H^s(-a,a))$, and, endowed with the norm

$$\|v\|_{Y_s} = \left(\int_{-a}^{a} \|v(\cdot,z)\|^2_{H^s(-a,a)}\, dz\right)^{1/2}, \tag{3.5}$$

Y_s is a Hilbert space. For $s = 1/2$, define, similarly, the Hilbert space

$$Y_{1/2} = L^2(-a,a;H^{1/2}_{00}(-a,a)). \tag{3.6}$$

Theorem 3.4 ([15]). *For every $s \in [0,1)$, the operator H_0 is linear and continuous from X into Y_s.*

Note that this result holds as well for the blurred projection operator $H = BH_0 = K \star H_0$. Note also that other regularity properties have been derived in [15], but the previous theorem is particularly useful in view of taking benefit of the Hilbert structure.

3.2.2. Minimization problem in fractional Sobolev spaces. Based on the functional properties stated in Theorem 3.4, we proposed to consider the following minimization problem. Let $s \in [0,1)$, let α and β be nonnegative real numbers, and let $\varepsilon > 0$. The projected image v_d (observed data) is assumed to belong to Y_s. Consider the problem of minimizing

$$F^s_{\alpha,\beta,\varepsilon}(u) = \frac{1}{2}\|Hu - v_d\|^2_{Y_s} + \alpha TV(u) + \frac{\beta}{2}\|u\|^2_X + \frac{1}{2\varepsilon}\|u - u^2\|^2_{L^2(\Omega)} \quad (3.7)$$

among all functions $u \in X$ where $\mathcal{X} = X = L^2(-a,a; BV_0(0,a))$ whenever $\alpha = 0$, and $\mathcal{X} = \mathrm{BV}(\Omega) \cap X$ whenever $\alpha > 0$.

Remark 3.1. *In fact the minimum of $F^s_{\alpha,\beta,\varepsilon}$ should be found among all functions $u \in \mathcal{B}_\eta$ where $\eta > 0$ and*

$$\mathcal{B}_\eta := \{\, u \in \mathcal{X} \mid \beta\|u\|_X + \|u\|_\infty \le \eta \,\}.$$

Indeed, because of the lack of coercivity of the functional we need a boundedness constraint to prove existence result within the infinite dimensional framework. However, we are allowed to choose any (large enough) η and the solution to the original (non penalized) problem exists without any additional condition. Therefore, from the practical point of view, this constraint will be inactive and we do not take it into account for numerical purpose.

The parameter α is the weight of the total variation. If $\alpha > 0$ then this term yields a regularization term used in a standard way in image processing. Note here that we introduce an alternative to this usual regularization, with the term $\|u\|^2_X$, weighted with β. Note that in our method it is required that $\alpha + \beta > 0$, that is, if $\alpha = 0$ then β must be chosen positive, and conversely. Note that $F^s_{\alpha,\beta,\varepsilon}$ is not differentiable because of these terms.

The parameter $\varepsilon > 0$ is a penalization parameter. The limit case $\varepsilon = 0$ corresponds to the binary constraint $u(r,z) \in \{0,1\}$ a.e. on Ω, and for this limit case it has been proved in [15] that the associated minimization problem has at least one solution. It has been proved as well that the minimization problem (3.7) is well defined and has at least one solution whenever $\varepsilon > 0$, and this family of optimization problems parameterized by ε enjoys a nice Γ-convergence property to the limit case.

First-order necessary conditions for optimality of (3.7) have also been derived in the form of an optimality system, as explained next. Although $F^s_{\alpha,\beta,\varepsilon}$ is not differentiable, the functional defined by

$$G^s(u) = \frac{1}{2}\|Hu - v_d\|^2_{Y_s} \quad (3.8)$$

is differentiable, and in what follows we denote by $\nabla G^s(u)$ its gradient for the pivot space L^2. It can be computed in several ways, in particular using a fractional Laplacian or using the Fourier transform. This will lead to different numerical implementation methods. The functional $u \mapsto \frac{1}{2\varepsilon}\|u - u^2\|^2_{L^2(\Omega)}$ is differentiable as well, and its gradient for the pivot space L^2 is

$$q_\varepsilon(u) = \frac{(u-u^2)(1-2u)}{\varepsilon}. \tag{3.9}$$

Recall that $X = L^2(-a,a;BV_0(0,a))$, and thus $X' = L^2(-a,a;(BV_0(0,a))')$. For every $\lambda \in X'$, viewed as function of $z \in (-a,a)$ of class L^2 with values in $(BV_0(0,a))'$, denote $\lambda_z = \lambda(z) \in (BV_0(0,a))'$, for almost every $z \in (-a,a)$. The duality product between X and X' is defined by

$$\langle \lambda, v\rangle_{X',X} = \int_{-a}^{a} \langle \lambda_z, v_z\rangle_{BV_0',BV_0}\, dz,$$

for every $\lambda \in X'$ and every $v \in X$. Finally, recall that the notation $TV_1(f)$ is used to denote the total variation of a function $f \in BV(0,a)$.

Theorem 3.5 ([15]). *Let u be a minimizer of (3.7) with the constraint $u \in \mathcal{B}_\eta$. Then there exist $\rho \in (\mathcal{M}(\Omega)^2)'$, $\mu = -div\ \rho$, and $\lambda \in X'$, such that*

$$\nabla G^s(u) + q_\varepsilon(u) + \alpha\mu + \beta\lambda = 0, \tag{3.10}$$

$$\mu \in \partial TV(u), \tag{3.11}$$

and

$$\lambda_z \in TV_1(u_z)\,\partial TV_1(u_z), \tag{3.12}$$

for almost every $z \in (-a,a)$.

4. Numerical implementation

4.1. Resolution of problem $(\mathcal{P}_\varepsilon)$

To solve the original problem, many numerical experiments are proposed in the literature. Usually, people use the back-filtered projection method (see Fig.4.1 below. In this case, results are of bad quality, as explained in [4]. In [1], the problem is studied via a shape optimization method. The object is viewed as a domain which optimal shape turns to be a solution. A derivative of the functional with respect to the domain is performed and a level-set method [38] is used. With this method, an Hamilton-Jacobi equation involving non local terms has to be solved. The use of classical finite difference schemes gives acceptable results (see Fig.4.2) but the method is time-consuming and highly unstable.

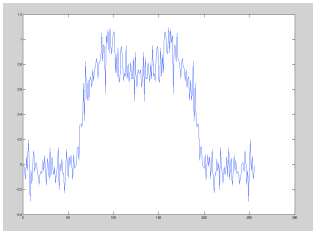

(a) Median line of the object ($i = 128$).

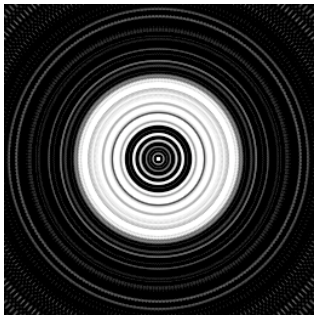

(b) Largest slice of the binary axially symmetric object by a plane orthogonal to the symmetry axis.

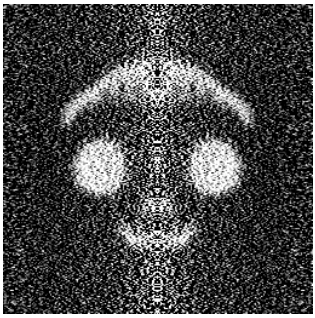

(c) Result using the cropped Ram-Lak filter.

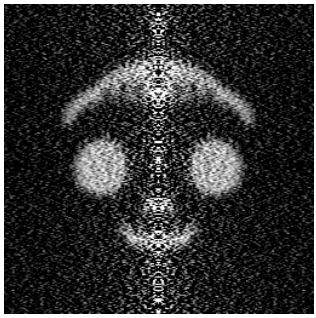

(d) Result using the Ram-Lak filter with a Hamming window.

FIGURE 4.1. Back-filtered projection results

(a) Synthetic object

(b) Computed solution

FIGURE 4.2. Level-set method results

An alternative *indirect method* has been tested in [4]. A solution to the first order optimality system of Theorem 3.3 has been computed . The results are good (see Fig.4.3) but the parameters tuning is quite delicate. In addition, though the computation time is much shorter than the methods mentioned before, it remains quite long.

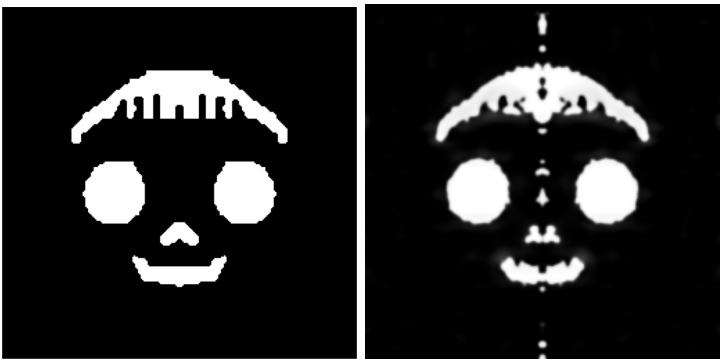

(a) Synthetic object (b) Computed solution

FIGURE 4.3. Penalization indirect method [4]

A more efficient, direct method has been described in [13]. Figure 4.4 shows what we may obtain. We refer to the quoted paper for more details.

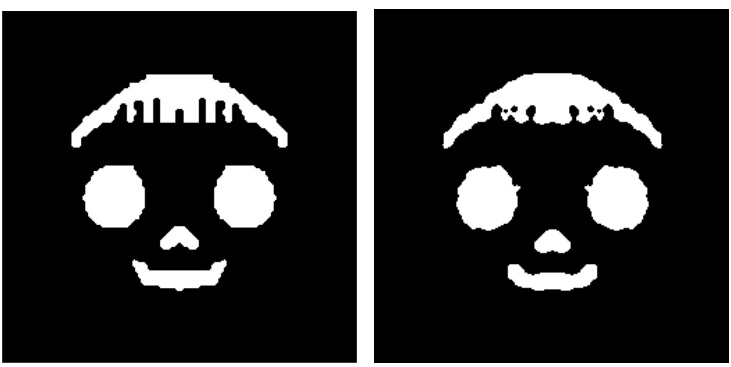

(a) The real object u. (b) Solution

FIGURE 4.4. Solution with a direct method [13]

4.2. Use of fractional optimality system

4.2.1. The general algorithm. In this section we explain how to carry out the numerical implementation of the optimality necessary conditions stated in Theorem 3.5. Notice that the method will depend on the four parameters

s, α, β, and ε. Their respective role will be explained and discussed further. These parameters being fixed, we propose the following iterative algorithm.

Algorithm 1

Initialization : $n = 0$, choose $u^0 = H_0^{-1} v_d$.
N_∞ maximum number of iterations.
Iterations :
for $0 \leq n \leq N_\infty$ **do**
(a) Determine $\mu^n \in \partial TV(u^n)$.
(b) Determine $\lambda_z^n \in TV_1(u_z^n)\, \partial TV_1(u_z^n)$, for every discretized value of $z \in (-a, a)$.
(c) Make p fixed-point-like iterations for the solving of

$$\nabla G^s(u^{n+1}) + q_\varepsilon(u^{n+1}) + \alpha\mu^n + \beta\lambda^n = 0.$$

(d) Stopping criterion: $|F^s_{\alpha,\beta,\varepsilon}(u^{n+1}) - F^s_{\alpha,\beta,\varepsilon}(u^n)|$ small enough
end for

We next discuss the discretization process, the steps of that algorithm, and the different implementation choices that can be done.

Discretization process. As usually, the discretized image is represented by a $N \times N$ array. Due to the symmetry, it suffices to deal with half an image, of size $N \times N/2$. Denote $X = \mathbb{R}^{N \times N}$ and $Y = X \times X$, endowed with the usual scalar product. For $u \in X$, the approximation of the Radon measure Du is identified with a vector of Y of coordinates $(Du)_{i,j} = ((Du)^1_{i,j}, (Du)^2_{i,j})$ defined by

$$(Du)^1_{i,j} = \begin{cases} u_{i+1,j} - u_{i,j} & \text{if} \quad i < N, \\ 0 & \text{if} \quad i = N, \end{cases} \quad (Du)^2_{i,j} = \begin{cases} u_{1,j+1} - u_{i,j} & \text{if} \quad j < N, \\ 0 & \text{if} \quad j = N, \end{cases}$$

and the approximation of total variation is

$$TV(u) = \sum_{1 \leq i,j \leq N} \sqrt{((Du)^1_{i,j})^2 + ((Du)^2_{i,j})^2}.$$

The divergence operator is discretized through

$$(\text{div } p)_{i,j} = \begin{cases} p^1_{i,j} - p^1_{i-1,j} & \text{if} \quad 1 < i < N \\ p^1_{i,j} & \text{if} \quad i = 1 \\ -p^1_{i-1,j} & \text{if} \quad i = N \end{cases} + \begin{cases} p^2_{i,j} - p^2_{i,j-1} & \text{if} \quad 1 < j < N \\ p^2_{i,j} & \text{if} \quad j = 1 \\ -p^2_{i,j-1} & \text{if} \quad j = N \end{cases}$$

Initialization. It is natural to initialize the algorithm with $u^0 = H_0^{-1} v_d$, that is, by applying the inverse of the (discretized) Radon transform to the observed data. As mentioned previously, the resulting image u^0 cannot be expected to be a nice reconstruction of the object (see also numerical simulations further), since it is far too much noised and blurred, however is the most natural initial point of our iterative procedure. A random initialization could

do not lead to a satisfying reconstruction since, in some sense, our algorithm acts as denoising and debluring.

Subdifferential of the total variation. The choice of $\mu \in \partial TV(u)$ or $\lambda_z \in TV_1(u_z)\,\partial TV_1(u_z)$ in (3.11)-(3.1b) follows Chambolle's method (see [21]). We briefly recall the idea for the construction of $\mu \in \partial TV(u)$ in the discretized setting. Recall that the Fenchel-Legendre conjugate function TV^* of TV is the indicator function $1_{\mathcal{K}_2}$ of

$$\mathcal{K}_2 = \{\text{div } g \mid g \in Y,\ (g^1_{i,j})^2 + (g^2_{i,j})^2 \leq 1,\ \forall i,j\}.$$

Moreover,

$$\mu \in \partial TV(u) \Leftrightarrow u \in \partial 1_{\mathcal{K}_2}(\mu) \Leftrightarrow \mu = \Pi_{\mathcal{K}_2}(\mu + u)$$

where $\Pi_{\mathcal{K}_2}$ denotes the orthogonal projection on $\mathcal{K}_2$. Therefore, μ can be computed with the successive approximation process $\mu_k = \Pi_{\mathcal{K}_2}(\mu_{k-1} + u)$ or with a semi-smooth Newton method. Similarly, for every discretized value of $z \in (-a, a)$., we compute $\lambda_z \in TV_1(u_z)\,\partial TV_1(u_z)$ as

$$\lambda_z = TV_1 i(u_z)\tilde{\lambda}_z \text{ with } \tilde{\lambda}_z = \Pi_{\mathcal{K}_1}(\tilde{\lambda}_z + u_z)$$

and

$$\mathcal{K}_1 = \{g' \mid g \in \mathbb{R}^N \times \mathbb{R}^N,\ (g^1_i)^2 + (g^2_i)^2 \leq 1,\ \forall i\}.$$

Therefore, $\tilde{\lambda}_z$ can also be computed with the successive approximation process $(\tilde{\lambda}_z)_k = \Pi_{\mathcal{K}_1}((\tilde{\lambda}_z)_{k-1} + u_z)$. The projected element $\bar{v} := \Pi_{\mathcal{K}_i}(v) = \text{div } \bar{p}$ where $\bar{p} = \text{argmin } \{ \| \text{div } (p) - v\|^2_X \mid |p_{i,j}| \leq 1,\ i,j = 1, \cdots, N \}$, may be computed using primal-dual or proximal methods for example.

Fixed-point-like iterations. In order to solve the third step of the iterative loop, we propose to implement a certain number of steps of a fixed-point-like iteration solving, as follows.

Given μ^n and λ^n, define $f^n(u) = \nabla G^s(u) + q_\varepsilon(u) + \alpha\mu^n + \beta\lambda^n$. The aim is to estimate u^{n+1} by solving the implicit nonlinear system $f^n(u) = 0$. This is equivalent to seeking u such that

$$u - M^n f^n(u) = u, \tag{4.1}$$

where M^n is a square (preconditioning) matrix to be chosen. We propose here to implement p steps of such a fixed-point procedure initialized at u^n, and the resulting solution is defined to be u^{n+1}. In practice, it happens to be sufficient to take $p = 1$, that is, we implement only one step of this fixed-point procedure.

A standard choice of preconditioner is $M^n = \gamma\,\text{Id}$, with $\gamma > 0$ small enough. This is however not the choice we make. Note that one recovers the classical Newton method whenever one chooses, at each step of the iteration, the matrix M^n to be the inverse of the differential of f^n at the current point. The classical Newton methods is a priori not well adapted here. Indeed, on the one part the discretization of the Radon transform is ill-conditioned, and hence the Hessian of G^s will be ill-conditioned as well, for every possible choice of the discretization of G^s (see further for different ways of computing the gradient of G^s). On the other part, the derivative of

the function q_ε defined by (3.9), seen as a function of one scalar variable, is $q_\varepsilon(t) = \frac{1}{\varepsilon}(2t-1)(t^2-t)$, and has three zeros: 0, 0.5, and 1. The classical Newton method for determining the zeros of that scalar function is written as

$$t_{k+1} = t_k - \frac{q_\varepsilon(t_k)}{q'_\varepsilon(t_k)}.$$

However the three zeros are attractive (see Figure 4.5), and in particular the attractive zero $t = 0.5$ should be avoided. Although this analysis is done in dimension 1, when transposed to imaging, a pixel coded with 0.5 is grey, exactly between 0 (black) and 1 (white), but our image is binary and this situation must be avoided. A very simple way, that we can explain in dimension 1, is to modify the classical Newton method so as to make the zero $t = 0.5$ repulsive. Due to the specific expression of the function $q_\varepsilon(\cdot)$, we propose to modify the classical Newton method as follows:

$$t_{k+1} = t_k - 2\frac{q_\varepsilon(t_k)}{|q'_\varepsilon(t_k)|}. \tag{4.2}$$

Let us justify this modification. Define Q_ε the primitive function of q_ε that vanishes at $t = 0$. Then we look for the minima of Q_ε on $[0,1]$. A descent method with optimal step α_k gives

$$t_{k+1} = t_k - \alpha_k q_\varepsilon(t_k);$$

a classical second order expansion gives

$$Q_\varepsilon(t_{k+1}) - Q_\varepsilon(t_k) = -\alpha_k(q_\varepsilon(t_k))^2 + \frac{\alpha_k^2}{2}(q_\varepsilon(t_k))^2 q'_\varepsilon(t_k) + \circ((t_{k+1}-t_k)^2)\ .$$

The first order analysis gives $\alpha_k > 0$ to let the functional decrease to a local minimum (here 0 or 1). Looking for a second order scheme gives

$$-\alpha_k(q_\varepsilon(t_k))^2 + \frac{\alpha_k^2}{2}(q_\varepsilon(t_k))^2 q'_\varepsilon(t_k) = 0,$$

that is $\alpha_k q'_\varepsilon(t_k) = 2$ which is equivalent to $\alpha_k = 2/|q'_\varepsilon(t_k)|$ since $\alpha_k > 0$.

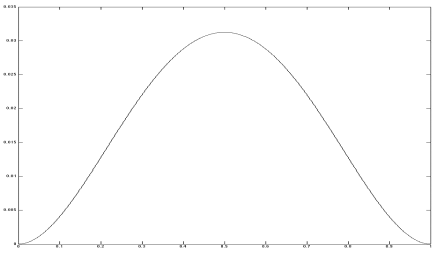

FIGURE 4.5. Graph of the primitive Q_ε of q_ε: $t \mapsto Q_\varepsilon(t)$

It is then obvious that, on this particular one-dimensional problem, this method is globally convergent, whatever the initialization t_0 may be (except

for three particular values). More precisely, for every $t_0 < 1/2$ such that $t_0 \neq \frac{1}{2} - \frac{1}{2\sqrt{3}}$, the iterative sequence (4.2) initialized at t_0 converges to 0, and for every $t_0 > 1/2$ such that $t_0 \neq \frac{1}{2} + \frac{1}{2\sqrt{3}}$, the iterative sequence (4.2) initialized at t_0 converges to 1. The two particular values $\frac{1}{2} \pm \frac{1}{2\sqrt{3}}$ correspond to the local extrema of the function $q_\varepsilon(\cdot)$, and actually, numerically they even do not cause the divergence of the above method. Indeed, due to the change of sign in (4.2), and for instance in the case $t_0 = \frac{1}{2} + \frac{1}{2\sqrt{3}}$, then numerically t_1 is set to a very large value, and then the next iterates will converge to 1, as expected.

We propose here to transpose this very simple idea to choose an adequate preconditioning matrix M^n for the solving of (4.1). As explained previously, since it suffices to work with half an image, u^n is a matrix of size $N \times N/2$. Then, the matrix $q'_\varepsilon(u^n)$ is as well of size $N \times N/2$, the lines of which are denoted by $L_1(u^n), \ldots, L_N(u^n)$. Then, guided by our one-dimensional analysis, we propose to consider as a matrix M^n, the diagonal $N \times N$-matrix having as diagonal i^{th}-coefficient the scalar $1/\|L_i(u^n)\|$ (using the Euclidean norm). Other choices are of course possible, but this specific choice happens to be the most relevant for our numerical simulations.

We are not able to provide a global convergence rate for Algorithm (4.2.1). However, the partial computations involve second order schemes and point fixed methods with projections. Therefore, we expect a linear convergence rate.

The previous analysis has been done with fixed parameters. In addition, we may give error estimates for the computed solution with respect to ε and α and/or β as well. For sake of simplicity we set $\beta = 0$. Indeed, we have noticed very small influence of β (see next section). Following [31], we introduce the $\mathcal{R}$-minimizing solution of the problem as

$$u^\dagger := \ \text{argmin}\{\mathcal{R}(u), Hu = u_d\ \},$$

where $\mathcal{R}(u) := TV(u) + \|u - u^2\|^2_{L^2(\Omega)}$. As H is surjective, equation $Hu = u_d$ has at least a solution and such a $\mathcal{R}$-minimizer exists. Following Remark 4.5 of [31] and considering that the appropriate assumptions are satisfied, we get

$$\|Hu_\alpha - u_d\|_{Y_s} \leq C\alpha \text{ and } D_{\xi^*}(u_\alpha, u^\dagger) \leq C\alpha\ ,$$

where C is a generic constant, u_α is a minimizer of $F^s_{\alpha,0,1/\alpha}$, $\xi^* \in \partial\mathcal{R}(u^\dagger)$ and $D_{\xi^*}(u_\alpha, u^\dagger)$ is the Bregman-distance :

$$D_{\xi^*}(u_\alpha, u^\dagger) = \mathcal{R}(u_\alpha) - \mathcal{R}(u^\dagger) - < \xi^*, u_\alpha - u^\dagger > \ .$$

4.2.2. Computation of the fractional derivative ∇G^s. It remains to explain how to compute a good approximation of the gradient ∇G^s. This is the most important issue of our algorithm, in the sense that all previous issues discussed above can be modified but variants lead to quite similar results (both in quality and execution time), whereas the choice of the numerical computation of ∇G^s leads to significant differences. Recall that the functional G^s defined by (3.8) is the square of the norm of the fractional-order Hilbert

space Y_s defined by (3.4). We next propose two numerical approaches to estimate such a norm and ∇G^s. The first one uses the Fourier transform and the second one uses an approximation of the fractional Laplacian. Whereas the first one may be expected to be more exact, actually the second one happens to be more relevant for the numerical simulations.

Using the Fourier transform. In this section, we compute ∇G^s using the Fourier transform. First of all, observe that, for every $s \in [0,1)$, for every $u \in Y_s$, the function $Hu - v_d$ can be extended by 0 to a function of $L^2(-a,a;H^s(\mathbb{R}))$, and its norm can be computed in terms of Fourier transform, by

$$\begin{aligned} G^s(u) &= \frac{1}{2}\int_{-a}^{a}\int_{\mathbb{R}} |\mathcal{F}_y(Hu - v_d)(\xi,z)|^2(1+\xi^2)^s \, d\xi \, dz \\ &= \frac{1}{2}\|\mathcal{F}_y(Hu - v_d)\|^2_{L^2(\omega_s)}, \end{aligned}$$

where $L^2(\omega_s)$ denotes the weighted Hilbertian space of all complex valued functions f defined on $\mathbb{R}\times(-a,a)$ such that $\int_{\mathbb{R}\times(-a,a)} |f(\xi,z)|^2\omega_s(\xi)\,d\xi\,dz < +\infty$, where $\omega_s(\xi) = (1+\xi^2)^s$. Setting $w_d = H^{-1}(v_d)$, it follows that

$$\nabla G^s(u) = (\mathcal{F}_y H)^* \omega_s (\mathcal{F}_y H)(u - w_d), \tag{4.3}$$

with L^2 as a pivot space. Moreover, in order to make this expression more explicit, the Fourier transform of the blurred projection operator H can be computed as follows (see [15]). The notation $\tilde{v}$ stands for the extension by 0 to $\mathbb{R}^2$ of any function v. Here it is assumed that the blur is modeled by a linear operator B writing as a convolution with a positive symmetric kernel K (in practice, a Gaussian kernel) with compact support.

Lemma 4.1. *The Fourier transform of the blurred projection operator $H = BH_0$ with respect to the first variable is*

$$(\mathcal{F}_y B\widetilde{H_0 u})(\xi,z) = (\mathcal{F}_y K)(\xi,\cdot) \star_2 (\mathcal{F}_y \widetilde{H_0 u})(\xi,\cdot)(z), \tag{4.4}$$

for every $u \in L^1(\Omega)$, every $\xi \in \mathbb{R}$ and almost every $z \in (-a,a)$, where the notation $\star_2$ stands for the convolution product with respect to the second variable. Its adjoint (with L^2 as a pivot space) is

$$((\mathcal{F}_y B\widetilde{H_0}^* v)(r,z) = (\mathcal{F}_y \widetilde{H_0})^*(\mathcal{F}_y g \star_2 v)(r,z), \tag{4.5}$$

for every $v \in L^1(\mathbb{R}^2)$, every $r \in [0,a)$ and almost every $z \in (-a,a)$.

Using the fractional Laplacian. In this section, we compute ∇G^s using the fractional Laplacian. By definition, there holds

$$G^s(u) = \frac{1}{2}\int_{-a}^{a} \|(Hu - v_d)(\cdot,z)\|^2_{H_0^s(-a,a)} dz,$$

for every $u \in Y_s$, and every $s \in [0,1)\setminus\{1/2\}$. For $s = 1/2$, $H_0^s(-a,a)$ is replaced with the Lions-Magenes space $H_{00}^{1/2}(-a,a)$. This norm can actually be expressed in an equivalent way using the fractional Laplacian operator, as follows (see [15] for the proofs). For every $f \in H_0^s(-a,a)$ whenever $s \in$

$[0,1) \setminus \{1/2\}$, or $f \in H_{00}^{1/2}(-a,a)$ whenever $s = 1/2$, the square of the norm of f within these spaces is equivalent to $\|f\|^2_{L^2(U)} + \|(-\Delta)^{s/2} f\|^2_{L^2(\mathbb{R}^n)}$, where f is extended by 0 outside $(-a,a)$ (notice that $(-\Delta)^{s/2} f$ is not of compact support[1]). Here, $(-\Delta)^\alpha$ denotes the fractional Laplacian operator on $\mathbb{R}^n$, defined, using the Fourier transform $\mathcal{F}f$ of f, by $(-\Delta)^\alpha f = \mathcal{F}^{-1}(|\xi|^{2\alpha}\mathcal{F}f)$. It follows that

$$\nabla G^s(u) = H^* R_{\Omega_1}(\mathrm{id} + (-\Delta)^s)(\widetilde{Hu} - \widetilde{v_d}), \tag{4.6}$$

with L^2 as a pivot space, where $\widetilde{Hu} - \widetilde{v_d}$ is the extension of $Hu - v_d$ by 0 outside $(-a,a)$, and R_{Ω_1} is the restriction to Ω_1.

It is very simple to approximate the operator $(-\Delta)^s$. To this aim, consider any usual approximation of the operator $-\Delta$, typically, the tridiagonal matrix

$$N^2 \begin{pmatrix} 2 & -1 & 0 & \cdots & 0 \\ -1 & 2 & -1 & & \vdots \\ 0 & -1 & 2 & \ddots & 0 \\ \vdots & & \ddots & \ddots & -1 \\ 0 & \cdots & 0 & -1 & 2 \end{pmatrix}. \tag{4.7}$$

Since it is a symmetric positive definite matrix, its fractional powers can be computed in many ways, for instance it is straightforward by considering its singular value decomposition (SVD). Note that this computation is done a priori and thus does not slow down the execution of the algorithm. There are some other ways to approximate the Laplacian operator, using higher-order centered schemes, but these variants do not lead to significant differences in the numerical simulations.

4.2.3. Numerical results. We present hereafter several numerical results using the synthetic object of Figure 3.1. In our numerical simulations, we consider a Gaussian blur with standard deviation $\sigma_B = 0.12$, that is, modeled by a convolution with the kernel

$$K(x) = Ce^{-\frac{|x|^2}{2\sigma_B^2}} 1_{\tilde{\Omega}}(x),$$

where C is a normalizing constant so that $\int K d\mu = 1$. The noise is assumed to be a Gaussian noise τ with standard deviation $\sigma_\tau = 0.15$ (the image is

[1]Note that the Laplacian operator should not be confused with the operator A defined as the opposite of the Dirichlet Laplacian on $L^2(-a,a)$, of domain $D(A) = H_0^1(-a,a) \cap H^2(-a,a)$. For instance, for every $f \in H_0^s(-a,a)$ with $s \in (0,1) \setminus \{1/2\}$ (and $f \in H_{00}^{1/2}(-a,a)$ for $s = 1/2$), one has $f \in D(A^{s/2})$ and thus $A^{s/2} f \in L^2(-a,a)$ by definition, whereas $(-\Delta)^s f \in L^2(\mathbb{R}^n)$ (where f is extended by 0 outside $(-a,a)$) is not even of compact support. Recall that functions of $H_0^s(U)$ can be extended by 0 to $H^s(\mathbb{R}^n)$ for every $s \geq 0$ such that $s \notin \mathbb{N} + 1/2$; for $s = 1/2$ for instance, functions of $H_{00}^{1/2}(U)$ can be extended by 0 to $H^{1/2}(\mathbb{R}^n)$.

rescaled between 0 and 1), that is,

$$\tau(x) = \frac{1}{\sqrt{2\pi}\sigma_\tau} e^{-\frac{|x|^2}{2\sigma_\tau^2}}.$$

We define the Signal to Noise Ratio as

$$SNR(v) = 20 \log_{10} \left(\|u_o\|_{L^2} / \|u_o - u_c\|_{L^2} \right) \ ,$$

where u_o is the expected original image and u_c is the computed one. All numerical tests have been performed with the same data whose size was 256×256. For the noisy case (without blur) SNR= 2.66 and the SNR corresponding to the noisy and blurred data is 2.35 .

First, we have compared the methods of subsection 4.2.2 to compute ∇G_s. The most efficient is the use of the fractional laplacian. Indeed, the choice of Fourier transform leads to numerical instability together with bad reconstruction. This comes from the fact that the implementation of the FFT is not based on Bessel functions which are the natural special functions associated to the Radon transform. The use of exact formulas with Bessel functions gives better results but none was as good as the ones we obtained with the fractional laplacian.

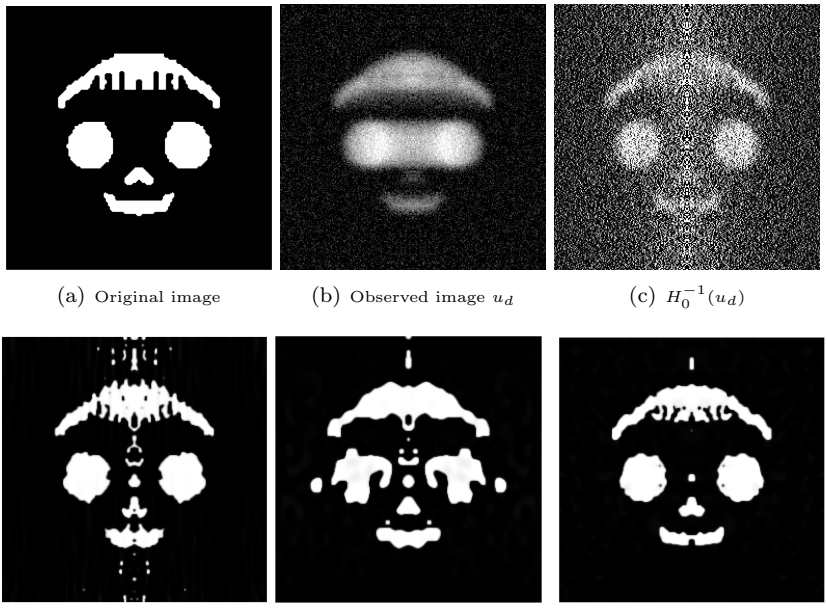

(a) Original image (b) Observed image u_d (c) $H_0^{-1}(u_d)$

(d) Use of exact formulas with Bessel functions (e) Use of FFT (f) Use of fractional laplacian

FIGURE 4.6. Results with Fractional approach : $s = 0.5$, $\varepsilon = 0.5, \alpha = 5, \beta = 0$

We have also tested the case where $\beta \neq 0$. If $\alpha = 0$ then the result is not satisfactory. If $\alpha \neq 0$ the effect of β is null. More numerical tests are available in [16]. Though we have improved the numerical method (using the fractional laplacian) the process is still not very fast. Therefore we use a wavelet approach that is described in next section.

4.3. Use of needlets

In this section, we describe an approach of smoothed Fourier series type based on a SVD type decomposition of the Radon projection operator H_0.

4.3.1. Abel integral and Jacobi based inversion formula. Let us start by observing that the Radon projection operator H_0 defined by (2.2) is related to the classical Abel integral transform $T_{1/2}u(x) = \int_0^x \frac{u(t)}{(x-t)^{1/2}}\,dt$ by the relation

$$H_0u(y,z) = \int_0^{1-|y|^2} u(\sqrt{1-t},z)\frac{1}{\sqrt{1-y^2-t}}\,dt = T_{1/2}\overline{u}_z(1-y^2),$$

where $\overline{u}_z(t) = u(\sqrt{1-t},z)$, for every $u \in \mathrm{BV}(\Omega)$.

For all $(\alpha,\beta) \in (-1,+\infty)^2$ and every $m \in \mathbb{N}$, let $J^{\alpha,\beta}_{[-1,1],m}$ denote the n-th degree Jacobi polynomial defined on $[-1,1]$, and let

$$J^{\alpha,\beta}_m(x) = \sqrt{\frac{n!(2n+\alpha+\beta+1)\Gamma(n+\alpha+\beta+1)}{\Gamma(n+\alpha+1)\Gamma(n+\beta+1)}}J^{\alpha,\beta}_{[-1,1],m}(2x-1),$$

for every $x \in [0,1]$. The family $(J^{\alpha,\beta}_n)_{m\in\mathbb{N}}$ is an Hilbertian basis of the (weighted) Hilbert space $L^2([0,1],(1-x)^\alpha x^\beta dx)$. In [7], the authors provide a SVD type decomposition of the operator $T_{1/2}$, showing in particular that

$$T_{1/2}(J^{0,0}_m)(x) = \beta_m x^\alpha J^{-1/2,1/2}_m(x),$$

for every $m \in \mathbb{N}$ and for every $x \in [0,1]$, where

$$\beta_m = \Gamma(1/2)\sqrt{\frac{\Gamma(m+1/2)}{\Gamma(m+3/2)}} \sim \frac{\Gamma(1/2)}{(m+3/2)^{1/2}}.$$

In terms of the Radon operator H_0, it follows that

$$H_0\left(J^{0,0}_m(1-r^2)g(z)\right)(y,z) = \beta_m\sqrt{1-y^2}J^{-1/2,1/2}_m(1-y^2)g(z)$$

for every function $g \in L^2(-1,1)$.

Let $Q_n(r) = J^{(0,0)}_m(1-r^2)$ and $Q^\#_m(y) = J^{(-1/2,1/2)}_m(1-y^2)$, by construction, $(Q_m)_{m\in\mathbb{N}}$ and $(Q^\#_m)_{m\in\mathbb{N}}$ are orthonormal bases of respectively $L^2(0,1,2rdr)$ and $L^2(0,1,2\sqrt{1-y^2}dy)$. Therefore any $u \in L^2(\Omega,2rdrdz)$ can be expanded along r as

$$u(r,z) = \sum_{m\in\mathbb{N}}\left(\int_0^1 u(r',z)Q_m(r')2r'dr'\right)Q_m(r')$$

and thus

$$H_0u(y,z) = \sum_{m\in\mathbb{N}} \left(\int_0^1 u(r',z) Q_m(r') 2r' dr' \right) \beta_m \sqrt{1-y^2} Q_m^{\#}(y)$$
$$= \sum_{m\in\mathbb{N}} \left(\int_0^1 H_0u(y',z) Q_m^{\#}(y') 2dy' \right) Q_m(r') \sqrt{1-y^2} Q_m^{\#}(y).$$

We derive thus the following one-dimensional inversion formula:

Lemma 4.2. *For every $u \in L^2(\Omega, 2rdrdz)$,*

$$u(r,z) = \sum_{m=0}^{+\infty} \frac{1}{\beta_m} \left(\int_0^1 (H_0u)(y',z) Q_m^{\#}(y') 2\, dy' \right) Q_m(r).$$

For any orthonormal basis of $L^2(-1,1)$ $(R_m)_{m\in\mathbb{N}}$, this formula yields a two-dimensional inversion formula:

Lemma 4.3. *For every $u \in L^2(\Omega, 2rdrdz)$,*

$$u(r,z) = \sum_{m=0}^{+\infty} \sum_{m'=0}^{+\infty} \frac{1}{\beta_m} \left(\int_{-1}^1 \int_0^1 (H_0u)(y',z') Q_m^{\#}(y') R_{m'}(z') 2\, dy' dz' \right) Q_m(r) R_{m'}(z).$$

Although the previous formula is valid for any orthogonal basis $(R_m)_{m\in\mathbb{N}}$, we will use in the following the choice $R_m = J_m^{(0,0)}$, i.e. the Legendre polynomial basis. This choice may seem arbitrary and unnecessarily complex. It turns out that the Legendre polynomial basis is nevertheless the simplest orthogonal basis of $L^2(-1,1)$ considered as an interval without any periodization. This polynomial basis has also, for any degree, some explicit cubature formula, a property which will proved to be important later on. A construction similar to the one proposed below could also be made with a Fourier basis but it suffers from periodization artifacts that are avoided by the choice of the Legendre polynomial basis.

4.3.2. Smoothed inversion and needlets. Assume now, as it is the case in practice, that we have only access to some approximations $\widetilde{h_{m,m'}}$ of

$$h_{m,m'} = \int_{-1}^1 \int_0^1 (H_0u)(y',z') Q_m^{\#}(y') R_{m'}(z') 2\, dy' dz'$$

for $0 \le m \le M$ and $0 \le m' \le M'$, how to use the previous formula to reconstruct an estimate of the function u?

Hard truncation, and Gibbs phenomenon. The most natural answer is to use the truncated reconstruction

$$\widetilde{P_{M,M'}u} = \sum_{m=0}^{M} \sum_{m'=0}^{M'} \frac{\widetilde{h_{m,m'}}}{\beta_m} Q_m(r') R_{m'}(z). \tag{4.8}$$

Although optimal from the quadratic risk point of view, this reconstruction however suffers from well known Gibbs type artifacts. Gibbs phenomena are well known in inverse problems and here in our tomography problem they

appear to be so strong that they make the use of such an inversion formula not suitable in the problem.

Smoothened truncation. As exemplified in [24] in the Fourier case and in [37] for Jacobi polynomials, there exists a simple method in order to cancel the Gibbs phenomenon. Let us recall this approach and show how it can be adapted and used in our context in a relevant way.

Let a be an arbitrary smooth nonnegative function supported in $[0,1]$, such that $a(w)=1$ for every $w\in[0,1/2]$ and $a(w)\leq 1$ for every $w\in(1/2,1]$. The method consists of replacing the hard truncation (4.8) with a soft one, by considering

$$\widetilde{P_{M,M'}}u(r)=\sum_{m=0}^{+\infty}\sum_{m'=0}^{+\infty}a\left(\frac{m}{M}\right)a\left(\frac{m'}{M'}\right)\frac{\widetilde{h_{m,m'}}}{\beta_m}Q_m(r)R_{m'}(z). \tag{4.9}$$

Note that the hard truncation would correspond to $a(w)=\chi_{[0,1]}(w)$. In Fourier series, the Fejer kernel corresponds to the choice $a(w)=\max(1-w,0)$ and is known to leads to better approximation. One can understand this smoothing effect through the study of the corresponding smoothed projector

$$P_{a,M,M'}u=\sum_{m=0}^{M}\sum_{m'=0}^{M}a\left(\frac{m}{M}\right)a\left(\frac{m'}{M'}\right)c_{m,m'}Q_m(r)R_{m'}(z).$$

with

$$c_{m,m'}=\int_0^1 u(r',z')Q_m(r')R_{m'}(z')2r'\,dr'dz'$$

Indeed, as soon as a is smooth, say $\mathcal{C}^\infty$, then those projectors satisfy some very nice properties, for instance all projections are now continuous for all L^p norms.

The best insight on those smoothened projection is probably the one proposed in [37]. Following their approach, the projection is first rewritten as a convolution

$$P_{a,M,M'}u=\int_{-1}^1 u(r',z')A_{a,M,M'}(r,z,r',z')2r'dr'dz'$$

with a kernel $A_{a,M,M'}$

$$A_{a,M,M'}(r,z,r',z')=\sum_{m=0}^{M}\sum_{m'=0}^{M'}a\left(\frac{m}{M}\right)a\left(\frac{m'}{M'}\right)Q_m(r)R_{m'}(z)Q_m(r')R_{m'}(z').$$

One of the main result of this section is to prove that if $a\in\mathcal{C}^\infty$ then this kernel is well localized spatially: for all $k\in\mathbb{N},\exists c_k>0$ such that

$$|A_{a,M,M'}(r,z,r',z')|\leq \frac{c_K MM'}{(1+Md(1-2r^2,1-2r'^2))^K(1+M'd(z,z'))^K\gamma(M,M',r,z,r',z')}$$

where $d(u,v) = |\arccos(u,v)|$ and

$$\gamma(M,M',r,z,r',z') = \sqrt{w_{0,0}(M,1-2r^2)w_{0,0}(M,1-2r'^2)w_{0,0}(M',z)w_{0,0}(M',z')}$$

with $w_{\alpha,\beta}(M,u) = (u+M^{-2})^{\alpha+1/2}(u-1+N^{-2})^{\beta+1/2}$. This result is sufficient to obtain the L^p continuity of the projection. Furthermore, one verify the existence of $c>1$ such that

$$\int_{-1}^{1}\int_{0}^{1} |P_{a,M,M'}u(r,z) - u(r,z)|^p \, 2rdrdz \leq c \inf_{v\in\mathcal{T}} \int_{-1}^{1}\int_{0}^{1} |v(r,z)-u(r,z)|^p \, 2rdrdz$$

where

$$\mathcal{T} := \mathrm{Span}\{Q_m(1-r^2)R_{m'}(z)\}_{0\leq m\leq M/2, 0\leq m'\leq M'/2} \ .$$

It turns out that this projection can be *discretized* as soon as there is a quadrature formula polynomials of finite degrees. Indeed, let Ξ_j be a set of quadrature point such that for any $Q_n(r)R_{n'}(z)$ and $Q_m(r)R_{m'}(z)$ with n, n', m and m' smaller than 2^j

$$\int_{-1}^{1}\int_{0}^{1} Q_n(r)R_{n'}(z)Q_m(r)R_{m'}(z)2rdrdz = \sum_{\xi=(r_\xi,z_\xi)\in\Xi_{2^j}} \omega_\xi Q_n(r_\xi)R_{n'}(z_\xi)Q_m(r_\xi)R_{m'}(z_\xi),$$

and define

$$\phi^{a,a}_{j,\xi}(r,z) = \sqrt{\omega_\xi}\sum_{m\in\mathbb{N}}\sum_{m'\in\mathbb{N}} \sqrt{a\left(\frac{m}{2^j}\right)a\left(\frac{m'}{2^j}\right)}Q_m(r_\xi)R_{m'}(z_\xi)Q_m(r)R_{m'}(z)$$

then

$$P_{a,2^j,2^j}u(r,z) = \sum_{\xi\in\Xi_j} d^{a,a}_{j,\xi}\phi^{a,a}_{j,\xi}(r,z)$$

with

$$d^{a,a}_{j,\xi} = \int_{-1}^{1}\int_{0}^{1} u(r',z')\phi^{a,a}_{j,\xi}(r',z')2r'dr'dz'.$$

Finally, if the quadrature points are chosen as the zeros of $Q_{2^{j+1}}(1-r^2)R_{2^{j+1}}(z)$ then forall $k\in\mathbb{N}, \exists c'_k$ such that

$$|\phi^{a,a}_{j,\xi}(r,z)| \leq \frac{c'_K 2^j}{(1+2^j d(1-2r^2,1-2r^2_\xi))^K(1+2^j d(z,z_\xi))^K\gamma(2^j,2^j,r,z,r_\xi,z_\xi)}.$$

Furthermore, $\forall p\in[1,+\infty], \exists(c_p,C_p,D_p)\in\mathbb{R}^3_{+,*}$ such that

$$\forall j\in\mathbb{N}, \forall\xi\in\Xi_j, c_p 2^{j(p/2-1)} \leq \int_{-1}^{1}\int_{0}^{1} |\phi^{a,a}_{j,\xi}(r,z)|^p 2rdrdz \leq C_p 2^{j(p/2-1)}$$

$$\forall d^{a,a}_{j,\xi}\in\mathbb{R}^{\Xi_j}, \int_{-1}^{1}\int_{0}^{1} |\sum_{\xi\in\Xi_j} d^{a,a}_{j,\xi}\phi^{a,a}_{j,\xi}(r,z)|^p 2rdrdz \leq C_p D_p 2^{j(p/2-1)}\sum_{\xi\in\Xi_j}|d^{a,a}_{j,\xi}|^p.$$

Needlets. The needlets corresponds to a multiscale representation associated to those projection. More precisely, for any $J > 0$

$$P_{a,2^J,2^J} = P_{a,1,1} + \sum_{j=1}^{J} \left(P_{a,2^j,2^j} - P_{a,2^{j-1},2^{j-1}} \right)$$

where by construction

$$P_{a,2^j,2^j} - P_{a,2^{j-1},2^{j-1}} u = \int_{-1}^{1} u(r',z') B_{a,2^j,2^j}(r,z,r',z') 2r' dr' dz'$$

with

$$B_{a,2^j,2^j}(r,z,r',z') =$$

$$\sum_{m=0}^{2^j} \sum_{m'=0}^{2^j} \left(a\left(\frac{m}{2^j}\right) a\left(\frac{m'}{2^j}\right) - a\left(\frac{m}{2^{j-1}}\right) a\left(\frac{m'}{2^{j-1}}\right) \right) Q_m(r) R_{m'}(z) Q_m(r') R_{m'}(z').$$

So that if we let $b(w) = a(w) - a(2w)$ and use

$$a(w)a(w') = a(2w)a(2w') + a(w)b(w') + b(w)a(w') + b(w')b(w')$$

$$\begin{aligned} B_{a,2^j,2^j}(r,z,r',z') = & \sum_{m=0}^{2^j} \sum_{m'=0}^{2^j} a\left(\frac{m}{2^j}\right) b\left(\frac{m'}{2^j}\right) Q_m(r) R_{m'}(z) Q_m(r') R_{m'}(z') \\ & + \sum_{m=0}^{2^j} \sum_{m'=0}^{2^j} b\left(\frac{m}{2^j}\right) a\left(\frac{m'}{2^j}\right) Q_m(r) R_{m'}(z) Q_m(r') R_{m'}(z') \\ & + \sum_{m=0}^{2^j} \sum_{m'=0}^{2^j} b\left(\frac{m}{2^j}\right) b\left(\frac{m'}{2^j}\right) Q_m(r) R_{m'}(z) Q_m(r') R_{m'}(z'). \end{aligned}$$

Using the cubature Ξ_j and defining the needlets

$$\psi^{b,a}_{j,\xi}(r,z) = \sqrt{\omega_\xi} \sum_{m\in\mathbb{N}} \sum_{m'\in\mathbb{N}} \sqrt{b\left(\frac{m}{2^j}\right) a\left(\frac{m'}{2^j}\right)} Q_m(r_\xi) R_{m'}(z_\xi) Q_m(r) R_{m'}(z)$$

$$\psi^{a,b}_{j,\xi}(r,z) = \sqrt{\omega_\xi} \sum_{m\in\mathbb{N}} \sum_{m'\in\mathbb{N}} \sqrt{a\left(\frac{m}{2^j}\right) b\left(\frac{m'}{2^j}\right)} Q_m(r_\xi) R_{m'}(z_\xi) Q_m(r) R_{m'}(z)$$

$$\psi^{b,b}_{j,\xi}(r,z) = \sqrt{\omega_\xi} \sum_{m\in\mathbb{N}} \sum_{m'\in\mathbb{B}} \sqrt{b\left(\frac{m}{2^j}\right) b\left(\frac{m'}{2^j}\right)} Q_m(r_\xi) R_{m'}(z_\xi) Q_m(r) R_{m'}(z),$$

one obtains

$$\left(P_{a,2^J,2^J} - P_{a,2^{J-1},2^{J-1}} \right) u = \sum_{o\in\{(a,b),(b,a),(b,b)} \sum_{\xi\in\Xi_J} d^o_{j,\xi}) \psi^o_{J,\xi}$$

with

$$d^o_{j,\xi} \int_{-1}^{1} \int_{0}^{1} u(r',z') \psi^o_{j,\xi}(r',z') 2r' dr' dz'.$$

Summing those equality over J yields

$$P_{a,2^J,2^J} u = \sum_{\xi\in\Xi_0} a_{j,\xi} \phi^{a,a}_{0,\xi} + \sum_{o\in\{(a,b),(b,a),(b,b)} \sum_{j=0}^{J} \sum_{\xi\in\Xi_j} d^o_{j,\xi} \psi^{a,b}_{j,\xi}$$

which implies that

$$\left\{\phi^{a,a}_{1,\xi}\right\}_{\xi\in\Xi_0}\cup\bigcup_{j\geq 0}\bigcup_{o\in\{(a,b),(b,a),(b,b)\}}\left\{\psi^{o}_{2^j,\xi}\right\}_{\xi\in\Xi_j}$$

is a tight frame.

Again, if the quadrature points are chosen as the zeros of $Q_{2^{j+1}}(1-r^2)R_{2^{j+1}}(z)$ then forall $k\in\mathbb{N},\exists c'_k$ such that

$$|\psi^o_{j,\xi}(r,z)|\leq\frac{c'_K 2^j}{(1+2^j d(1-2r^2,1-2r_\xi^2))^K(1+2^j d(z,z_\xi))^K\gamma(2^j,2^j,r,z,r_\xi,z_\xi)}.$$

Furthermore, $\forall p\in[1,+\infty],\exists(c_p,C_p,D_p)\in\mathbb{R}^3_{+,*}$ such that

$$\forall j\in\mathbb{N},\forall\xi\in\Xi_j,c_p 2^{j(p/2-1)}\leq\int_{-1}^1\int_0^1|\psi^o_{j,\xi}(r,z)|^p 2rdrdz\leq C_p 2^{j(p/2-1)}$$

$$\forall d^o_{j,\xi}\in\mathbb{R}^{3\times\Xi_j}\int_{-1}^1\int_0^1|\sum_o\sum_{\xi\in\Xi_j}d^o_{j,\xi}\psi^o_{j,\xi}(r,z)|^p 2rdrdz\leq C_pD_p2^{j(p/2-1)}\sum_o\sum_{\xi\in\Xi_j}|d^o_{j,\xi}|^p.$$

This implies that the L^p norm of u can be controlled through the needlet coefficients and thus that it suffices to well estimate the needlet coefficients to well estimate the function.

Needlet coefficient estimation. To produce a good estimate of u, it suffices thus to produce good estimates for the needlet coefficients:

$$\int_{-1}^1\int_0^1 u(r',z')\psi^o_{j,\xi}(r',z')2r'dr'dz'.$$

Using the definition, one has for $\psi^o_{j,\xi}$:

$$\begin{aligned}
d^o_{j,\xi}&=\int_{-1}^1\int_0^1 u(r,z)\psi^o_{j,\xi}(r,z)2rdrdz\\
&=\int_{-1}^1\int_0^1 u(r,z)\left(\sqrt{\omega_\xi}\sum_{m\in\mathbb{N}}\sum_{m'\in\mathbb{N}}\sqrt{o_1\left(\frac{m}{2^j}\right)o_2\left(\frac{m'}{2^j}\right)}Q_m(r_\xi)R_{m'}(z_\xi)Q_m(r)R^{(0,0)}_{m'}(z)\right)2rdrdz'\\
&=\sqrt{\omega_\xi}\sum_{m\in\mathbb{N}}\sum_{m'\in\mathbb{N}}\sqrt{o_1\left(\frac{m}{2^j}\right)o_2\left(\frac{m'}{2^j}\right)}Q_m(r_\xi)R_{m'}(z_\xi)\left(\int_{-1}^1\int_0^1 u(r,z)Q_m(r)R_{m'}(z)2rdrdz\right)\\
&=\sqrt{\omega_\xi}\sum_{m\in\mathbb{N}}\sum_{m'\in\mathbb{N}}\sqrt{o_1\left(\frac{m}{2^j}\right)o_2\left(\frac{m'}{2^j}\right)}Q_m(r_\xi)R_{m'}(z_\xi)\frac{h_{m,m'}}{\beta_m}.
\end{aligned}$$

A natural estimate for $d^o_{j,\xi}$ is thus given by

$$\widetilde{d^o_{j,\xi}}=\sqrt{\omega_\xi}\sum_{m\in\mathbb{N}}\sum_{m'\in\mathbb{N}}\sqrt{o_1\left(\frac{m}{2^j}\right)o_2\left(\frac{m'}{2^j}\right)}Q_m(r_\xi)R_{m'}(z_\xi)\frac{\widetilde{h_{m,m'}}}{\beta_m}.$$

Note that by construction

$$\begin{aligned}
\widetilde{P_{a,2^J,2^J}}u&=\sum_{\xi\in\Xi_0}\widetilde{d^{a,a}_{0,\xi}}\phi^{a,a}_{0,\xi}+\sum_{j=0}^J\sum_o\sum_{\xi\in\Xi_j}\widetilde{d^o_{j,\xi}}\psi^0_{j,xi}\\
&=\sum_{n=0}^{2^J}\sum_{n'=0}^{2^J}a\left(\frac{n}{2^J}\right)a\left(\frac{n'}{2^J}\right)\frac{\widetilde{h_{n,n'}}}{\beta_n}Q_n(r)R_{n'}(z)
\end{aligned}$$

and thus the needlets seem not to be useful as the second formula is simpler.

It turns out that this estimate can be transformed in a better one in terms of expected error by thresholding the estimated coefficients, i.e. replacing them by 0 when they are small. This idea has been introduced by Donoho et al in statistics and relies on approximation theory. It is based on the observation that if a needlet coefficient $d^o_{j,\xi}$ of the true function u is small with respect to the approximation error between $d^o_{j,\xi}$ and $\widetilde{d^o_{j,\xi}}$ then it is better to replace the approximated value by 0. This idea can not be used as is as the value of $d^o_{j,\xi}$ is unknown but it is replaced by a decision based on a comparison between the approximation $\widetilde{d^o_{j,\xi}}$ and a threshold $T_{j,\xi}$ meant as an expected error term. This yields the thresholding estimate

$$\widetilde{u}_J = \sum_{\xi\in\Xi_0} \widetilde{d^{a,a}_{0,\xi}}\phi^{a,a}_{0,\xi} + \sum_{j=0}^{J}\sum_{o}\sum_{\xi\in\Xi_j} \rho_{T_{j,\xi}}\left(\widetilde{d^o_{j,\xi}}\right)\psi^0_{j,xi}$$

with $\rho_T(x) = x$ if $|x| > T$ and 0 otherwise and $T_{j,\xi}$ is a family of threshold to be chosen. For instance, in a Gaussian white noise framework, $T_{j,\xi}$ is chosen as a multiple of the expected standard deviation. As soon as there is some blurring, the inversion formula (4.3) does not hold anymore. Following ideas of [35], we propose to simply apply a regularized inverse operator B_ρ^{-1} to the noisy observation $v_d = BH_0u+\tau$ and apply the thresholded needlet estimator to $B_\rho^{-1}v_d$. The choice of the thresholds depends on the specific inverse used as is it set to the expected standard deviation of the coefficients of the noise after the application of the regularized inverse.

Algorithm 2

Initialization : Compute $I_d = B_\rho^{-1}v_d$ - $n = 0$
Iterations :
for $0 \le n, b' \le 2^J$ **do**

Compute $h_{n,n'} = \dfrac{8}{2^{2J}}\displaystyle\sum_{i=1}^{N/2}\sum_{j=1}^{N} I_d[i,j]Q_n^{\#}(2i/N)R_{n'}(i/N-1)$

end for
For $\xi \in \Xi_0$, compute $d^{a,a}_{0,\xi} = \dfrac{h_{0,0}}{\beta_0}Q_0(r_\xi)R_0(z_\xi)$
for $0 \le j \le J$ **do**
For $\xi \in \Xi_j$, for all o, compute

$$\widetilde{d^o_{j,\xi}} = \sqrt{\omega_\xi}\sum_{n=0}^{2^j}\sum_{n'=0}^{2^j}\sqrt{o_1\left(\frac{n}{2^j}\right)o_2\left(\frac{n'}{2^j}\right)}Q_n(r_\xi)R_{n'}(z_\xi)\widetilde{\frac{h_{n,n'}}{\beta_n}}$$

and $\rho_{T_{j,\xi}}(\widetilde{d^o_{j,\xi}})$
end for
Set $\widetilde{u}^{Th} = \displaystyle\sum_{\xi\in\Xi_0} \widetilde{d^{a,a}_{0,\xi}}\phi^{a,a}_{0,\xi} + \sum_{j=0}^{J}\sum_{o}\sum_{\xi\in\Xi_j} \rho_{T_{j,\xi}}\left(\widetilde{d^o_{j,\xi}}\right)\psi^0_{j,xi}$
where $v_d[i,j] = v_d(2i/N, i/N-1)$.

Such an algorithm gives similar results to the ones in Figure 4.6(f). There is no great improvement in terms of SNR for example. However, the computational time is widely reduced.

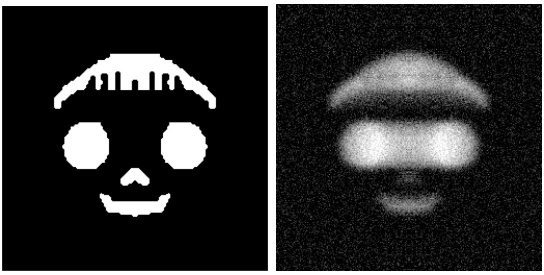

(a) Original image (b) Observed image u_d

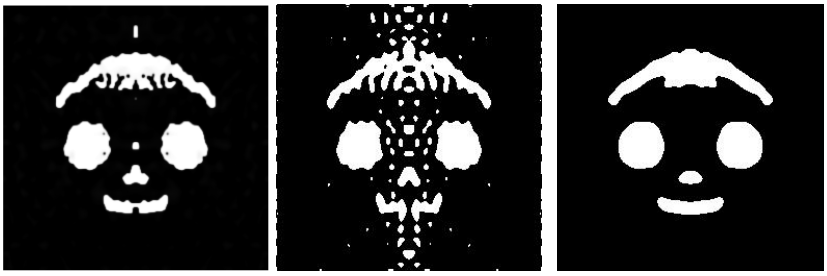

(c) Fractional laplacian reconstruction, $\varepsilon = 0.5,\ \alpha = 5,\ \beta = 0$ (d) Smooth truncated Needlet reconstruction (e) Threshold Needlet reconstruction

FIGURE 4.7. Results with Needlet approach

5. Non axially symmetric objects : optimal transport approach

Next, we abandon the axially symmetry assumption but we use the previous results. Indeed, we assume that a first guess of the object has been reconstructed, for example with the previous techniques and we would like to move this initial object to the solution which is not assumed to be axially symmetric any longer.
In what follows, $\{\theta_0, \theta_1, \ldots, \theta_{p-1}\}$ denotes the p acquisition angles (in $[0, \pi[$). The measured data are $\pi_i (:= H_i \rho) \in L^2(\tilde{\Omega})$ where $H_i := H_{\theta_i},\ i = 0, \cdots, p-1$. The (open) set Ω is now a subset of $\mathbb{R}^d$ and $\tilde{\Omega} \subset \mathbb{R}^{d-1}$.

We first used an elastic model (optical flow) to achieve this goal. As we will see, this is not satisfactory enough and we decided to use optimal transport techniques.

5.1. An elastic model

5.1.1. Presenting the model. We assume that we know an initial object ρ_0 that we may compute (for example) as a radially symmetric object with the mean value of the p projections.
We want to find a deformation vector field $g : \rho_0 \mapsto \rho$ that moves ρ_0 to ρ the so-called solution which fits the projection data:

$$\left\{ \begin{array}{lll} g: & \bar{\Omega} \subset \mathbb{R}^d & \to \bar{\Omega} \\ & x & \mapsto g(x) = (g_1(x), \cdots, g_d(x)) \end{array} \right.$$

We call Φ the map that provides the solution ; precisely

$$\forall g \qquad \Phi(g) = \rho_0 \circ (\mathrm{Id} + g) \ ,$$

where Id is the identity operator in $\mathbb{R}^d$. Then, the fitting data term writes

$$F(g) := \sum_{k=0}^{p-1} \int_\Omega (H_k \Phi(g) - \pi_k)^2(x) dx \ ,$$

and we define the cost functional as

$$J(g) = \frac{1}{2} F(g) + \frac{\lambda+\mu}{2} \|\mathrm{div}\ g\|_{L^2}^2 + \frac{\mu}{2} \|\nabla g\|_{(L^2)^d}^2,$$

where λ and μ are the Lamé coefficients that describe the body deformations and $\nabla g = (\nabla g_1, \cdots, \nabla g_d)$. Next we consider the optimization problem

$$\min_{g \in \mathcal{B}} J(g) \tag{$\mathcal{P}$}$$

where $\mathcal{B}$ is the vector space of admissible vector fields, for instance

$$\mathcal{B} := \{ g : \bar{\Omega} \to \bar{\Omega} \mid \mathrm{supp}\ \Phi(g) \subset \bar{\Omega} \} \ .$$

We briefly and formally describe the method.
The Euler equation writes $\nabla_g J(g^*) = 0$ if g^* is a solution. A classical computation gives

$$\sum_{k=0}^{p-1} H_k^* [H_k \Phi(g^*) - \pi_k] \nabla_x \Phi(g^*) - (\lambda+\mu) \nabla(\mathrm{div}\ g^*) - \mu \Delta g^* = 0,$$

or equivalently

$$\forall i = 1, \cdots, d \qquad \sum_{k=0}^{p-1} H_k^* (H_k \rho_0 (I + g^*) - \pi_k) \frac{\partial \rho_0 (I+g^*)}{\partial x_i} - (\lambda+\mu) \frac{\partial (\mathrm{div}\ g^*)}{\partial x_i} - \mu \Delta g_i^* = 0.$$

In addition we have to prevent $\Phi(g^*)$ to have a support outside $\bar{\Omega}$, so we add the (vectorial) boundary condition

$$\frac{\partial g}{\partial n} = 0 \ .$$

5.1.2. Numerical realization. The algorithm is devoted to the computation of a solution to the Euler equation $\Psi(g^*) = 0$ with a descent method and Ψ is given by (5.1)

$$\Psi(g) = (\lambda+\mu) \nabla(\mathrm{div}\ g) + \mu \Delta g - \sum_{k=0}^{p-1} H_k^* [H_k \Phi(g) - \pi_k] \nabla_x \Phi(g). \tag{5.1}$$

We set $d = 2$ and $\Omega =]-a, a[\times]-a, a[$ as an example. The discretization process is standard (see Section 4.2). Let us precise the discrete form of the projection operators in the case where we have three angles : $\theta_0 = 0$, $\theta_1 = \dfrac{\pi}{2}$ and $\theta_2 = \dfrac{\pi}{4}$. Recall that

$$H_\theta \rho(y) = \int_{-\infty}^{+\infty} 1_\Omega(x, y) \rho(x \cos\theta + y \sin\theta, -x \sin\theta + y \cos\theta)\, dx.$$

A straight forward computation gives

$$\forall \ell \in \{1, \cdots, N\} \qquad H_0 \rho(y_\ell) \simeq H_0 \rho(\ell) := \sum_{k=1}^{N} M_{k,\ell}\, \rho(k, \ell) \ . \tag{5.2}$$

where $h = 2a/N$ and

$$M_{k,\ell} = \begin{cases} h & \text{if } x_k^2 + y_\ell^2 \leq a^2 \\ 0 & \text{else} \end{cases} = h \begin{cases} 1 & \text{if } (2k-N)^2 + (2\ell - N)^2 \leq N^2 \\ 0 & \text{else} \end{cases}$$

and in the case where $\theta = \dfrac{\pi}{2}$

$$\forall k \in \{1, \cdots, N\} \qquad H_1\rho(x_k) \simeq H_1\rho(k) := \sum_{\ell=1}^{N} M_{\ell,k}\, \rho(k,\ell)\ . \tag{5.3}$$

In the case $\theta = \dfrac{\pi}{4}$, the detector has to be discretized in a different way because it is not parallel to the axis of the cartesian grid. We finally obtain

$$\forall \ell \in \{1, \cdots, 2N-1\} \qquad H_2\rho(z_\ell) \simeq H_2\rho(\ell) := \sum_{k=1}^{N} \widetilde{M}_{k,l}\, \rho(k, \ell - k)\ . \tag{5.4}$$

where we have set for every $\ell \in \{1, \cdots, 2N-1\}$ and $k \in \{1, \cdots, N\}$

$$\begin{aligned} \widetilde{M}_{k,\ell} &= \begin{cases} h\sqrt{2} & \text{if } |\ell - 2k| \leq \sqrt{\frac{N^2}{2} - (\ell - N)^2} \text{ and } \ell \in \mathcal{I}_N \\ 0 & \text{else} \end{cases} \\ &= h\sqrt{2} \begin{cases} 1 & \text{if } (2k-\ell)^2 + (\ell - N)^2 \leq \frac{N^2}{2} \\ 0 & \text{else} \end{cases} \end{aligned}$$

Similarly the discrete form of the adjoint operators writes: $\forall k, \ell \in \{1, \cdots, N\}$

$$(H_0^* w)(k,\ell) = M_{k,\ell}\, w(\ell),\ (H_1^* w)(k,\ell) = M_{\ell,k}\, w(k), (H_2^* w)(k,\ell) = \widetilde{M}_{k,\ell+k}\, w(\ell + k).$$

Note that it is usually assumed that $h = 1$ (and $a = N/2$) in image processing. For more details one can refer to [2].

Algorithm 3

Initialization : $n = 0$, $g^0 = 0$. Choose τ (descent parameter)
N_∞ maximum number of iterations.
Iterations :
for $0 \leq n \leq N_\infty$ **do**
(a) Compute.

$$\Psi^n = (\lambda + \mu)\nabla(\text{div } g^n) + \mu \Delta g^n - \sum_{k=0}^{p-1} H_k^*[H_k\Phi(g^n) - \pi_k]\nabla_x \Phi(g^n)$$

(b) $g^{n+1} = g^n + \tau \Psi^n$.
end for

The results are not very good: the tuning the parameters λ and μ is delicate. If they are too large the algorithm diverges.The solution looks as it was noisy (though a small τ seems to have a denoising effect) and overall the process is quite slow. Of course, the numerical method could be improved a lot. However, we decided to investigate another approach, using optimal transport theory.

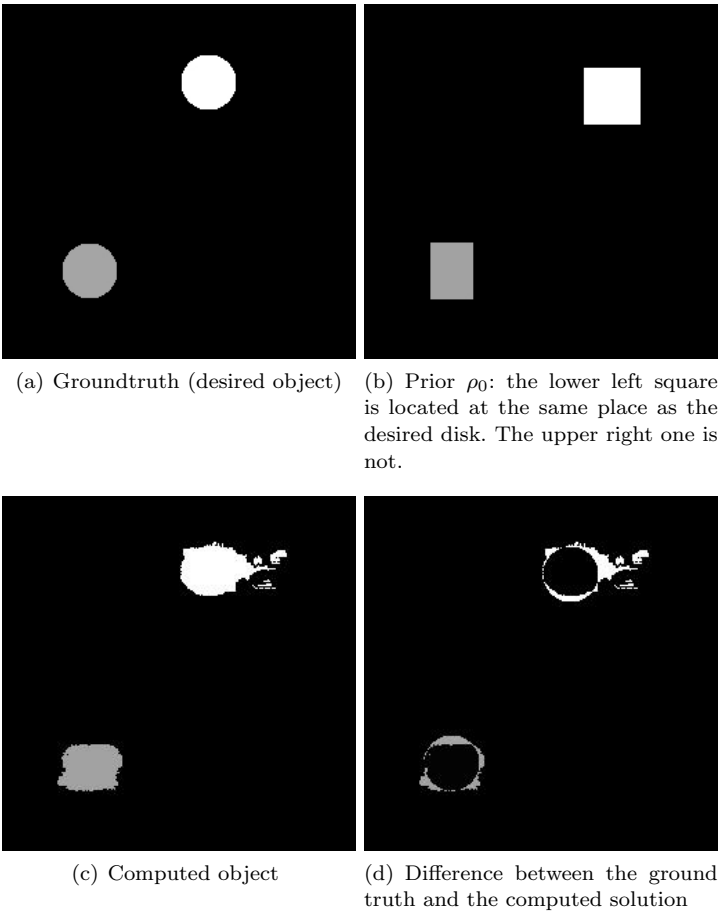

(a) Groundtruth (desired object)

(b) Prior ρ_0: the lower left square is located at the same place as the desired disk. The upper right one is not.

(c) Computed object

(d) Difference between the ground truth and the computed solution

FIGURE 5.1. Results with $\lambda = 0.1, \mu = 0.1$ and $\tau = 0.5$ - 1000 iterations

5.2. Optimal transport model : multi-marginal approach

5.2.1. Presenting the model. We first suppose that the studied object is described by a function (with compact support) $f : \mathbb{R}^d \longmapsto \mathbb{R}$ that gives the attenuation coefficient of the material at the current point, and we set $\rho(d\mathbf{x}) = cf(\mathbf{x})d\mathbf{x}$ where c is a normalizing constant so that ρ is a probability measure on $\mathbb{R}^d$ (we denote by bold letters the vectors and by regular ones the real numbers). In what follows, we want to recover ρ from the data and some prior, and we will search ρ in the set of probability measures on $\mathbb{R}^d$ (with finite second moments).

The data of tomographic reconstruction problem are

- a set of unitary directions $\mathbf{r}_i \in S^{d-1}$, $i = 1, \dots k$, where S^{d-1} denotes the unit ball of $\mathbb{R}^{d-1}$, corresponding to the X-ray propagation directions.
- a corresponding collection of probability measures π_i, $i = 1, \dots, k$ respectively defined on $\mathbf{r}_i^{\perp}$, with finite second moments.

The probability π_i represents the X-ray measurement on a hyperplane $\mathbf{r_i}^\perp$. Note that if $d = 2$ this hyperplane reduces to a line. In this case, we set $\mathbf{d}_i := \mathbf{r_i}^\perp \in S^1$, a generating direction. For the sake of mathematical generality we present the model in $\mathbb{R}^d$ while keeping 1D projections. The probability π_i represents now the X-ray measurement on a line whose direction is $\mathbf{d_i}$. Let us denote by $\Pi_{\mathbf{d_i}}$ the projection operator on the line directed by $\mathbf{d_i}$ and by and by $T_\#\mu$ the push-forward of the measure μ through the map T: T is a map from $\mathbb{R}^n$ to $\mathbb{R}^p$, such that for every Borel subset A of $\mathbb{R}^p$ $T_\#\mu(A) = \mu(T^{-1}(A))$.Then, without noise perturbation, , we have

$$\pi_i = \Pi_{\mathbf{d}_i\#}\rho$$

or equivalently, for every continuous function φ on $\mathbb{R}$ with compact support

$$\int_{\mathbb{R}} \varphi(t)\pi_i(dt) = \int_{\mathbb{R}^d} \varphi(\mathbf{d}_i \cdot \mathbf{x})\rho(d\mathbf{x}).$$

As said before, the measure ρ is not uniquely determined by these few projections and we must add some additional assumption to be able to perform the desired reconstruction. Again, we suppose that we have a prior ρ_0 and that the real object ρ is *close* to this prior. We are looking for a probability measure ρ whose transportation cost from ρ_0 is small and whose projections match the data π_i. As these data are noisy, this matching cannot be perfect and we introduce a variational model.

In the sequel, $\mathcal{P}_2(\mathbb{R}^d)$ (respectively $\mathcal{P}_2(\mathbb{R})$) will denote the set of probability measures on $\mathbb{R}^d$ ($\mathbb{R}$) with finite second moment. For μ and ν in $\mathcal{P}_2(\mathbb{R}^d)$, the squared-2-Wasserstein distance between μ and ν is by definition

$$W^2(\mu,\nu) := \inf_{\gamma\in\Gamma(\mu,\nu)} \int_{\mathbb{R}^d\times\mathbb{R}^d} |\mathbf{x}-\mathbf{y}|^2\gamma(d\mathbf{x},d\mathbf{y})$$

where $\Gamma(\mu,\nu)$ denotes the set of probability measures on $\mathbb{R}^d \times \mathbb{R}^d$ having μ and ν as marginals. The fact that the previous infimum is attained is classical, also, we recall a useful dual formula due to Kantorovich that enables one to express W^2 as

$$W^2(\mu,\nu) = \sup_{(f,g)\in C_b(\mathbb{R}^d)\times C_b(\mathbb{R}^d)} \left\{ \int_{\mathbb{R}^d} f d\mu + \int_{\mathbb{R}^d} g d\nu \ : \ f(\mathbf{x}) + g(\mathbf{y}) \le |\mathbf{x}-\mathbf{y}|^2 \right\}$$

Slightly abusing notations, we shall also use the notations W^2 for the squared 2-Wasserstein distance between probability measures on the real line and the notation $\Gamma(\mu,\nu)$ for the set of probability measures having μ and ν as marginals *even if μ and ν are probability measures on spaces with different dimensions.*

Given positive weights $\lambda_0, \lambda_1, \ldots, \lambda_k$, $\rho_0 \in \mathcal{P}_2(\mathbb{R}^d)$, and $\pi_i \in \mathcal{P}_2(\mathbb{R})$ for $i = 1, \ldots, k$, we consider as cost the weighted sum of squared 2-Wasserstein distances i.e.

$$J(\rho) := \frac{\lambda_0}{2} W^2(\rho_0,\rho) + \frac{1}{2}\sum_{i=1}^{k} \lambda_i W^2(\pi_i, \Pi_{\mathbf{d}_i\#}\rho).$$

For further use, let us remark that it is easy to see that one may express the one-dimensional squared 2-Wasserstein distance between π_i and $\Pi_{\mathbf{d}_i\#}\rho$ equivalently either as

$$W^2(\pi_i, \Pi_{\mathbf{d}_i\#}\rho) = \inf_{\gamma_i\in\Gamma(\pi_i,\Pi_{\mathbf{d}_i\#}\rho)} \int_{\mathbb{R}\times\mathbb{R}} (x_i - y_i)^2\gamma_i(dx_i,dy_i)$$

or

$$W^2(\pi_i, \Pi_{\mathbf{d}_i\#}\rho) = \inf_{\eta_i\in\Gamma(\pi_i,\rho)} \int_{\mathbb{R}\times\mathbb{R}^d} (x_i - \mathbf{x}\cdot\mathbf{d}_i)^2\eta_i(dx_i,d\mathbf{x}). \tag{5.5}$$

Our aim is to study the following (convex) minimization problem

$$\inf_{\rho\in\mathcal{P}_2(\mathbb{R}^d)} J(\rho). \tag{$\mathcal{P}$}$$

The direct method of the calculus of variations applies so that ($\mathcal{P}$) admits at least a minimizer. Let us present the dual formulation as in [5, 3] (in the $\mathcal{P}_2$ framework as in the present paper). Let f_0 be a real-valued function defined on $\mathbb{R}^d$; we then define $f_0^{\lambda_0}$ by the infimal convolution formula:

$$f_0^{\lambda_0}(\mathbf{x_0}) := \inf_{\mathbf{x}\in\mathbb{R}^d}\left\{\frac{\lambda_0}{2}|\mathbf{x_0}-\mathbf{x}|^2 - f_0(\mathbf{x})\right\},\ \forall \mathbf{x_0}\in\mathbb{R}^d\ . \tag{5.6}$$

In a similar way, for $f_i\colon \mathbb{R}\to\mathbb{R}$, we define

$$f_i^{\lambda_i}(x_i) := \inf_{y_i\in\mathbb{R}^d}\left\{\frac{\lambda_i}{2}(x_i-y_i)^2 - f_i(y_i)\right\},\ \forall x_i\in\mathbb{R}.$$

Then define

$$F(f_0,f_1,\dots,f_k) := \int_{\mathbb{R}^d} f_0^{\lambda_0}(\mathbf{x_0})\rho_0(d\mathbf{x_0}) + \sum_{i=1}^k \int_{\mathbb{R}} f_i^{\lambda_i}(x_i)\pi_i(dx_i)$$

and consider the (concave) maximization problem

$$\sup_{(f_0,\dots,f_k)\in K} F(f_0,f_1,\dots,f_k) \tag{$\mathcal{P}^*$}$$

where K consists of continuous functions that have at most quadratic growth at infinity and such that

$$f_0(\mathbf{x}) + \sum_{i=1}^k f_i(\mathbf{d}_i\cdot\mathbf{x}) = 0,\ \forall \mathbf{x}\in\mathbb{R}^d. \tag{5.7}$$

Then we have equivalence between the primal and dual problem in the following sense :

Theorem 5.1. *The following duality relation holds*

$$\inf(\mathcal{P}) = \sup(\mathcal{P}^*).$$

Moreover, ($\mathcal{P}^*$) admits a solution $(f_0,f_1,\dots,f_1)$ that can be chosen in such a way that the functions $v_1,\dots,v_k$ defined by

$$v_i(t) := \frac{\lambda_i}{2}t^2 - f_i(t),\ t\in\mathbb{R},\ i=1,\dots,k \tag{5.8}$$

are convex (which in particular implies that the functions $f_1,\dots,f_k$ can be chosen semiconcave on $\mathbb{R}$ and f_0 semiconvex on $\mathbb{R}^d$).

Next we are able to give an equivalent linear reformulation that takes the form of a multi-marginal optimal transport problem.
For any $\overline{\mathbf{x}} := (\mathbf{x_0},x_1,\dots,x_k)\in\mathbb{R}^d\times\mathbb{R}^k$, let us define

$$\overline{c}(\overline{\mathbf{x}}) := \inf_{\mathbf{x}\in\mathbb{R}^d}\left\{\frac{\lambda_0}{2}|\mathbf{x_0}-\mathbf{x}|^2 + \sum_{i=1}^k \frac{\lambda_i}{2}(x_i-\mathbf{x}\cdot\mathbf{d}_i)^2\right\}. \tag{5.9}$$

This quadratic problem has a unique minimizer that we denote $\overline{T}(\overline{\mathbf{x}})$; its expression is easy to compute and reads as

$$\overline{T}(\overline{\mathbf{x}}) = \left(\lambda_0\,\mathrm{id} + \sum_{i=1}^k \lambda_i \mathbf{d}_i\times\mathbf{d}_i\right)^{-1}(\lambda_0\mathbf{x_0} + \sum_{i=1}^k \lambda_i x_i\mathbf{d}_i). \tag{5.10}$$

Then, $\overline{c}(\overline{\mathbf{x}})$ writes

$$\overline{c}(\overline{\mathbf{x}}) = \frac{\lambda_0}{2}|\mathbf{x_0}|^2 + \sum_{i=1}^{k} \frac{\lambda_i}{2} x_i^2 - \frac{1}{2} A z(\overline{\mathbf{x}}) \cdot z(\overline{\mathbf{x}}) \tag{5.11}$$

with

$$A := \left(\lambda_0 \,\mathrm{id} + \sum_{i=1}^{k} \lambda_i \mathbf{d}_i \times \mathbf{d}_i \right)^{-1} \text{ and } z(\overline{\mathbf{x}}) := \lambda_0 \mathbf{x_0} + \sum_{i=1}^{k} \lambda_i x_i \mathbf{d}_i. \tag{5.12}$$

The multi-marginal optimal transport problem then reads

$$\inf_{\gamma \in \Gamma(\rho_0, \pi_1, \ldots, \pi_k)} \int_{\mathbb{R}^d \times \mathbb{R}^k} \overline{c}(\overline{\mathbf{x}}) \gamma(d\overline{\mathbf{x}}) \tag{$\mathcal{P}_m$}$$

where $\Gamma(\rho_0, \pi_1, \ldots, \pi_k)$ denotes the set of probability measures on $\mathbb{R}^d \times \mathbb{R}^k$ having $\rho_0, \pi_1, \ldots, \pi_k$ as marginals and $\overline{c}$ is the cost computed above. Again the existence of an optimal measure for ($\mathcal{P}_m$) is easy to prove and the connection between ($\mathcal{P}$) and ($\mathcal{P}_m$) is then given by

Theorem 5.2. *If $\overline{\gamma}$ solves ($\mathcal{P}_m$) then $\overline{\rho} := \overline{T}_{\#}\overline{\gamma}$ (where $\overline{T}$ given by (5.10)) solves ($\mathcal{P}$).*

Thank to expression (5.11), problem ($\mathcal{P}_m$) is equivalent to

$$\sup_{\gamma \in \Gamma(\rho_0, \pi_1, \ldots, \pi_k)} \frac{1}{2} \int_{\mathbb{R}^d \times \mathbb{R}^k} A z(\overline{\mathbf{x}}) \cdot z(\overline{\mathbf{x}}) \gamma(d\overline{\mathbf{x}}) \tag{5.13}$$

where the symmetric positive definite matrix A and the linear map z are defined in (5.12). Using ($\mathcal{P}_m$) dual formulation

$$\inf \left\{ \int_{\mathbb{R}^d} \mathbf{u}_0 \rho_0 + \sum_{i=1}^{k} \int_{\mathbb{R}} u_i \pi_i \,|\, \mathbf{u}_0(\mathbf{x_0}) + \sum_{i=1}^{k} u_i(x_i) \geq \frac{1}{2} A z(\overline{\mathbf{x}}) \cdot z(\overline{\mathbf{x}}),\ \forall \overline{\mathbf{x}} \in \mathbb{R}^d \times \mathbb{R}^k \right\} \tag{$\mathcal{P}_m^*$}$$

we can prove that, if γ is optimal for (5.13) and $(\mathbf{u}_0, u_1, \ldots, u_k)$ solves ($\mathcal{P}_m^*$), then for γ a.e. $\overline{\mathbf{x}} = (\mathbf{x_0}, x_1, \ldots, x_k)$ one has

$$\mathbf{u}_0(\mathbf{x_0}) + \sum_{i=1}^{k} u_i(x_i) = \frac{1}{2} A z(\overline{\mathbf{x}}) \cdot z(\overline{\mathbf{x}}).$$

If, in addition, $\mathbf{u}_0$ is differentiable at $\mathbf{x_0}$ and u_i is differentiable at x_i one has:

$$\nabla \mathbf{u}_0(\mathbf{x_0}) = \lambda_0 A z(\overline{\mathbf{x}}) \Rightarrow z(\overline{\mathbf{x}}) = \frac{A^{-1} \nabla \mathbf{u}_0(\mathbf{x_0})}{\lambda_0} \tag{5.14}$$

and

$$u_i'(x_i) = \lambda_i A z(\overline{\mathbf{x}}) \cdot \mathbf{d}_i = \frac{\lambda_i}{\lambda_0} \nabla \mathbf{u}_0(\mathbf{x_0}) \cdot \mathbf{d}_i \Rightarrow x_i = (u_i')^{-1} \Big(\frac{\lambda_i}{\lambda_0} \nabla \mathbf{u}_0(\mathbf{x_0}) \cdot \mathbf{d}_i \Big). \tag{5.15}$$

So, we may deduce the following result on uniqueness of the optimal measure γ for (5.13) and that it is of Monge type (i.e. supported by a graph over the $\mathbf{x_0}$ variable):

Theorem 5.3. *Assume that ρ_0 vanishes on small sets and that π_i does not charge points for $i = 1, \ldots, k$. Then (5.13) admits a unique solution γ that is of Monge-Type (i.e. induced by a map) and given by*

$$\gamma := \Psi_{\#}\rho_0$$

where

$$\Psi(\mathbf{x_0}) := \Big(\mathbf{x_0}, (u_1')^{-1} \Big(\frac{\lambda_1}{\lambda_0} \nabla \mathbf{u}_0(\mathbf{x_0}) \cdot \mathbf{d}_1 \Big), \ldots, (u_k')^{-1} \Big(\frac{\lambda_k}{\lambda_0} \nabla \mathbf{u}_0(\mathbf{x_0}) \cdot \mathbf{d}_k \Big) \Big)$$

and the strongly convex potentials $\mathbf{u}_0$, $u_1, \ldots, u_k$ solve the dual problem ($\mathcal{P}_m^*$).

Combining the previous with proposition 5.2 we obtain

Corollary 5.1. *Under the assumptions of theorem 5.3, the solution $\overline{\rho}$ of $(\mathcal{P})$ is of Monge type and given by*

$$\overline{\rho} = \overline{F}_{\#}\rho_0$$

where

$$\overline{F}(\mathbf{x_0}) := A\Big(\lambda_0\mathbf{x_0} + \sum_{i=1} \lambda_i (u_i')^{-1}\Big(\frac{\lambda_i}{\lambda_0}\nabla \mathbf{u}_0(\mathbf{x_0})\cdot \mathbf{d}_i\Big)\mathbf{d}_i\Big). \tag{5.16}$$

In the sequel (especially for numerical tests) we use a formulation derived from equations (5.15) and(5.16) as $\overline{F}(\mathbf{x_0}) = \mathbf{x_0} + \delta\mathbf{x}_0$, where $\delta\mathbf{x}_0$ stands for the displacement. Indeed, these two equations yield

$$A^{-1}(\overline{F}(\mathbf{x_0})) = A^{-1}(\mathbf{x_0} + \delta\mathbf{x}_0) = \lambda_0\mathbf{x_0} + \sum_{i=1}^{k} \lambda_i x_i\, \mathbf{d}_i\ .$$

With (5.12), we get $A^{-1}(\delta\mathbf{x}_0) + \sum_{i=1}^{k} \lambda_i(\mathbf{d}_i \times \mathbf{d}_i)\mathbf{x_0} = \sum_{i=1}^{k} \lambda_i x_i\, \mathbf{d}_i$ that is

$$A^{-1}(\delta\mathbf{x}_0) = \sum_{i=1}^{k} \lambda_i (x_i - \mathbf{x_0}\cdot\mathbf{d}_i)\mathbf{d}_i.$$

Finally

$$\overline{F}(\mathbf{x_0}) = \mathbf{x_0} + A\left(\sum_{i=1}^{k} \lambda_i (x_i - \mathbf{x_0}\cdot\mathbf{d}_i)\mathbf{d}_i\right). \tag{5.17}$$

Proceeding as in [3, 5], we deduce the following regularity result:

Theorem 5.4. *If, in addition to the assumptions of Theorem 5.3, ρ_0 belongs to $L^\infty(\mathbb{R}^d)$ then $\overline{\rho}$ belongs to $L^\infty(\mathbb{R}^d)$ as well.*

5.2.2. Numerical realization. The numerical realization is quite delicate and deserves a finer study (by comparing different points of view). What follows is rather a validation of the model than a complete numerical investigation.

Let us describe the numerical process to solve problem $(\mathcal{P}_m^*)$ (which involves the computation of only one infimal convolution, whereas $(\mathcal{P}^*)$ involves k of them)

$$\inf\left\{\int_{\mathbb{R}^d} \mathbf{u_0}\,\rho_0 + \sum_{i=1}^{k}\int_{\mathbb{R}} u_i\pi_i \ \mid\ \mathbf{u_0}(\mathbf{x_0}) + \sum_{i=1}^{k} u_i(x_i) \geq \frac{1}{2}A\overline{z}(\overline{\mathbf{x}})\cdot\overline{z}(\overline{\mathbf{x}}),\ \forall \overline{\mathbf{x}} \in \mathbb{R}^d\times\mathbb{R}^k\right\}$$

where $\mathbf{u} = (u_1, \cdots, u_k)$, $\mathbf{x} = (x_1, \cdots, x_k) \in \mathbb{R}^k$, $\overline{\mathbf{x}} = (\mathbf{x_0}, \mathbf{x}) \in \mathbb{R}^d \times \mathbb{R}^k$, A, and $z(\overline{\mathbf{x}})$ are defined by equations (5.11) and (5.12).

Problem $(\mathcal{P}_m^*)$ can be equivalently written as

$$\inf_{\mathbf{u}}\left\{\sum_{i=1}^{k}\int_{\mathbb{R}} u_i\pi_i - \int_{\mathbb{R}^d}\min_{\mathbf{x}\in\mathbb{R}^k}\left(\sum_{i=1}^{k} u_i(x_i) - \frac{1}{2}A\overline{z}(\mathbf{x_0},\mathbf{x})\cdot\overline{z}(\mathbf{x_0},\mathbf{x})\right)\rho_0(d\mathbf{x_0})\right\}. \tag{5.18}$$

We set

$$H(\mathbf{u},\mathbf{x_0},\mathbf{x}) = \sum_{i=1}^{k} u_i(x_i) - \frac{1}{2}A\overline{z}(\mathbf{x_0},\mathbf{x})\cdot\overline{z}(\mathbf{x_0},\mathbf{x})$$

and compute, if possible, a solution to

$$\min_{\mathbf{x}\in\mathbb{R}^k} H(\mathbf{u},\mathbf{x_0},\mathbf{x}). \tag{5.19}$$

Note that the existence and uniqueness of solutions is not a priori ensured. It depends on the behavior of the functions $\mathbf{u}$ with respect to the quadratic form $Az(\mathbf{x_0}, \mathbf{x}) \cdot z(\mathbf{x_0}, \mathbf{x})$. Indeed we know by the theory that the solution $\mathbf{u}$ is strongly convex. We must ensure coercivity for H. This will be the case if the strong convexity constant of $\mathbf{u}$ is greater that the one of the quadratic form. The latter is driven by the parameters $\lambda_i, i = 0, \cdots, k$. As the different directions $\mathbf{d}_i$ play the same role it is consistent to choose $\lambda_i = 1, i = 1, \cdots, k$. The only parameter to tune is $\lambda = \lambda_0$. For numerics we set $\lambda = 10^{-4}$.
Assuming that problem (5.19) has at least a solution $\mathbf{x}^*$ we may use Euler equation and set $\nabla_{\mathbf{x}} H(\mathbf{u}, \mathbf{x_0}, \mathbf{x}^*) = 0$. A short computation gives :

$$\forall i = 1, \cdots, k \qquad \frac{\partial H}{\partial x_i}(\mathbf{u}, \mathbf{x_0}, \mathbf{x}) = u_i'(x_i) - \lambda_i Az(\mathbf{x_0}, \mathbf{x}) \cdot \mathbf{d}_i.$$

Therefore the solution $\mathbf{x}^*(\mathbf{u}, \mathbf{x_0})$ is implicitly given by the following system :

$$\forall i = 1, \cdots, k \quad \frac{\partial H}{\partial x_i}(\mathbf{u}, \mathbf{x_0}, \mathbf{x}^*) = u_i'(x_i^*) - \lambda_i Az(\mathbf{x_0}, x_1^*, \cdots, x_k^*) \cdot \mathbf{d}_i = 0. \tag{5.20}$$

With (5.12) relation (5.20) writes:

$$\forall i = 1, \cdots, k \qquad u_i'(x_i^*) = \lambda_i \lambda_0 A\mathbf{x_0} \cdot \mathbf{d}_i + \sum_{p=1}^{k} \alpha_{i,p} x_p^*,$$

where we have set $\alpha_{i,p} = \lambda_p (A\mathbf{d}_p \cdot \mathbf{d}_i)$ for $i, p = 1, \cdots, k$. Setting $\mathbb{A} = (a_{i,p})_{i,p=1,\cdots,k}$ gives that $\mathbf{x}^*(\mathbf{u}, \mathbf{x_0})$ is solution of the following system

$$\forall i = 1, \cdots, k \quad u_i'(x_i^*) = \lambda_0 A\mathbf{x_0} \cdot (\lambda_i \mathbf{d}_i) + (\mathbb{A}x^*)_i. \tag{5.21}$$

Once $\mathbf{x}^*(\mathbf{u}, \mathbf{x_0})$ is computed, the cost functional in problem ($\mathcal{P}_m^*$) reads

$$\mathcal{J}(\mathbf{u}) = \sum_{i=1}^{k} \int_{\mathbb{R}} u_i \pi_i - \int_{\mathbb{R}^d} H(\mathbf{u}, \mathbf{x_0}, \mathbf{x}^*(\mathbf{u}, \mathbf{x_0})) \rho_0(d\mathbf{x_0}).$$

To use a numerical method to minimize $\mathcal{J}$, we have to compute $\nabla \mathcal{J}(\mathbf{u})$.
Let be $\varphi : \mathbb{R} \to \mathbb{R}$ and $i \in \{1, \cdots, k\}$:

$$\frac{\partial \mathcal{J}}{\partial u_i}(\mathbf{u}) \cdot \varphi = \int_{\mathbb{R}} \varphi \pi_i - \int_{\mathbb{R}^d} \left(\frac{\partial H}{\partial u_i}((\mathbf{u}, \mathbf{x_0}, \mathbf{x}^*(\mathbf{u}, \mathbf{x_0})) \cdot \varphi \right) \rho_0(d\mathbf{x_0}).$$

The computation of $\dfrac{\partial H}{\partial u_i}((\mathbf{u}, \mathbf{x_0}, \mathbf{x}^*) \cdot \varphi$ gives

$$\frac{\partial H}{\partial u_i}(\mathbf{u}, \mathbf{x_0}, \mathbf{x}^*) \cdot \varphi = \varphi(x_i^*) + \sum_{j=1}^{k} \frac{\partial H}{\partial x_j}(\mathbf{u}, \mathbf{x_0}, \mathbf{x}^*) \frac{\partial x_j^*}{\partial u_i}(\mathbf{u}, \mathbf{x_0}, \mathbf{x}^*) \cdot \varphi.$$

Therefore

$$\forall i = 1, \cdots, k \quad \frac{\partial \mathcal{J}}{\partial u_i}(\mathbf{u}) \cdot \varphi = \int_{\mathbb{R}} \varphi \pi_i - \int_{\mathbb{R}^d} \varphi(x_i^*(\mathbf{u}, \mathbf{x_0})) \rho_0(d\mathbf{x_0}), \tag{5.22}$$

where $\mathbf{x}^*(\mathbf{u}, \mathbf{x_0})$ satisfies (5.21).

We decided to use a Galerkin type method to approximate the solution. More precisely, we choose a suitable basis (FEM, spectral or spline) to write the function u. Here, we decided to use a spline basis, so that u is described by very few scalar coefficients. In addition, such an approach allows to compute the integral quantities once at the beginning of the process. The algorithm writes :

Algorithm 4

Given λ_i, $i = 0, \cdots, k$, $\mathbf{d}_i$, $i = 1, \cdots, k$.
Compute integrals ($\mathbf{x_0}$ and φ are known), A and $\mathbb{A}$.

Initialization : Choose $\mathbf{u}^0_{i=1..k}$ - $n = 0$ - N_∞ is the maximum number of iterations.

Iterations :

for $0 \leq n \leq N_\infty$ **do**

(a) Compute $\mathbf{x}^{*n}_{i=1..k}[\mathbf{u}^n_{i=1..k}, \mathbf{x_0}]$ solving

$$(u^n_{k,i})'(x^{*n}_{k,i}) - (\mathbb{A}x^{*n})_i = \lambda_0 A\mathbf{x_0} \cdot (\lambda_i \mathbf{d}_i);$$

(b) Compute $\nabla\mathcal{J}(\mathbf{u}^n_{i=1..k})$ with

$$\frac{\partial \mathcal{J}}{\partial u_j}(\mathbf{u}^n_{i=1..k}) = \pi_j - T_{j,k}\#\rho_0$$

where $T^n_{i=1..k}(\mathbf{x_0}) := x^{n*}_{i=1..k}(\mathbf{u}^n_{i=1..k}, \mathbf{x_0})$.

(c) Compute $\mathbf{u}^{n+1}_{i=1..k} = \mathbf{u}^n_{i=1..k} - \tau_k \nabla\mathcal{J}(\mathbf{u}^n_{i=1..k})$.

(c) Stopping criterion

end for

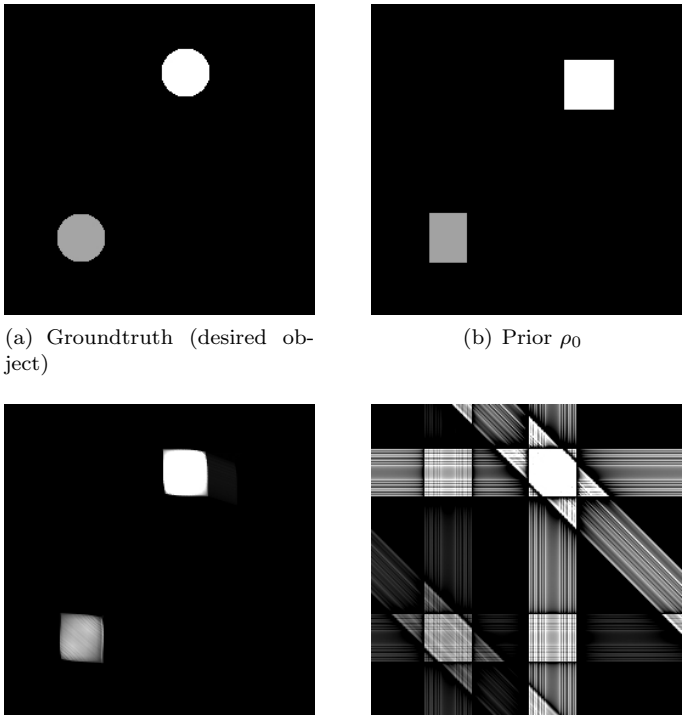

(a) Groundtruth (desired object)

(b) Prior ρ_0

(c) Computed object with optimal transport

(d) Computed object with the standard back-filtered projection algorithm

FIGURE 5.2. Example 1: no mass outside the two disks.

We present in Figures 5.2 and 5.3 two academic examples obtained with three views with directions $\mathbf{d}_1 = (1,0), \mathbf{d}_2 = (0,1),\ \mathbf{d}_3 = (1,-1)/\sqrt{2}$. In both cases $\lambda_i = 1,\ i = 1,2,3$ and $\lambda = 10^{-4}$. These examples seem similar. The prior ρ_0 is designed such that the lower left square is located at the same place as the desired disk. The upper right one is not. In Figure 5.2 (Example 1), we note in (c) that the squares have been moved at the right place (the centers of the disk and square are the same). However, the shapes do not fit well.

The main difference between the two examples is that the material density is not zero in example 2. So the induced mass will be transported as well : this is an undesirable effect that we see on Figure 5.3.

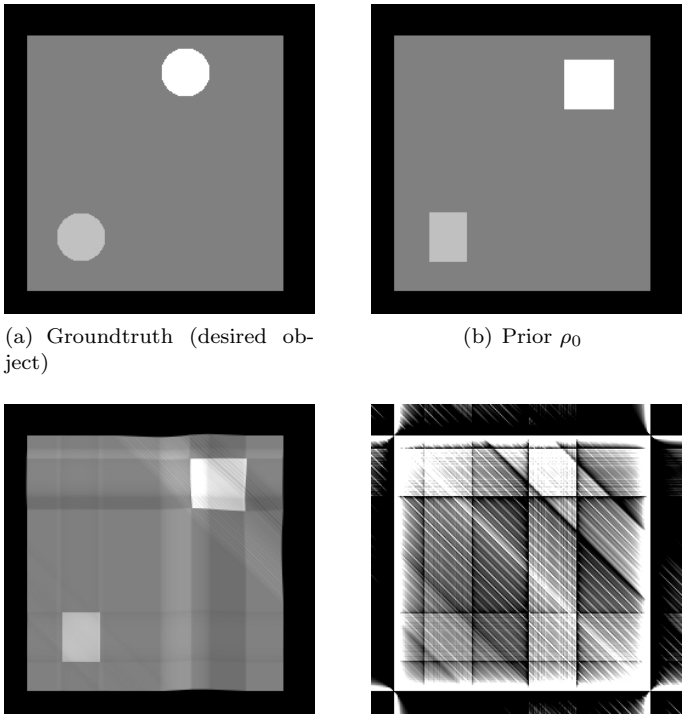

(a) Groundtruth (desired object)

(b) Prior ρ_0

(c) Computed object with optimal transport

(d) Computed object with the standard back-filtered projection algorithm

FIGURE 5.3. Example 2 : there is mass outside the two disks. We see in (c) that the whole band containing the square has been transported and not the square only. So, the upper right square is not located at it should be.

Recall that these results are extracted from [3] and more details can be found in that paper. Other numerical methods and/or formulations may be investigated using for example entropy regularization as in [12].

6. Conclusion

We have given an overview of the different methods we used to deal with that complicated problem. As we mentioned before, more comments, proofs and examples can be found in the quoted papers. We have not presented all the numerical methods and alternative models we have been investigating during the past decade but the papers appear in the references. Let us point out that results of sections 4.2 and 5.1 were unpublished.

The optimal transport approach seems promising. An alternative point of view using the partial differential transport equation and optimal control techniques is currently under investigation using the formulation of [11].

References

[1] I. Abraham, R. Abraham and M. Bergounioux, *An Active Curve Approach for Tomographic Reconstruction of Binary Radially Symmetric Objects* , Numerical Mathematics and Advanced Applications, Kunisch K. , Of G., Steinbac O. (Eds.), pp. 663-670 (2008).

[2] I. Abraham, R. Abraham, M. Bergounioux, *A variational method for tomographic reconstruction with few views,* http://hal.archives-ouvertes.fr/hal-00697218, April 2012.

[3] I. Abraham, R. Abraham, M. Bergounioux and G. Carlier, *Tomographic reconstruction from a few views: a multi-marginal optimal transport approach*, Applied Mathematics and Optimization, **75**, 1, 55–73 (2017).

[4] R. Abraham, M. Bergounioux and E. Trélat, *A penalization approach for tomographic reconstruction of binary radially symmetric objects*, Applied Mathematics and Optimization, **58**, 3, 345-371 (2008).

[5] M. Agueh and G. Carlier, *Barycenters in the Wasserstein space*, SIAM J. Math. An., **43**, 2, 904-924 (2011).

[6] L. Ambrosio, N. Fusco and D. Pallara, *Functions of bounded variation and free discontinuity problems*, Oxford mathematical monographs, Oxford University Press (2000).

[7] A. Ammar and A. Karoui, *Stable inversion of the Abel integral equation of the first kind by means of orthogonal polynomials*, Inverse Problems, **26**, 105005, 28 pp (2010).

[8] G. Ambartsoumian and P. Kuchment, *A range description for the planar circular Radon transform*, SIAM J. Math. Anal. **38** , 2, 681- 692 (2006).

[9] H. Attouch, G. Buttazzo, and G. Michaille, *Variational analysis in Sobolev and BV spaces*, MPS/SIAM Series on Optimization, Vol. 6, Society for Industrial and Applied Mathematics (SIAM), Philadelphia, PA, (2006).

[10] R.H.T. Bates, K.L. Garden and T.M. Peters, *Overview of computerized tomography with emphasis on future developments*, Proc. IEEE **71**, 3 , 356-297 (1983).

[11] J. D. Benamou and Y. Brenier *A computational fluid mechanics solution to the Monge-Kantorovich mass transfer problem* , Numerische Mathematik, **84**, 3, 375-393 (2000).

[12] J. D. Benamou, G. Carlier, M. Cuturi, L. Nenna and G. Peyré, *Iterative Bregman Projections for Regularized Transportation Problems*, SIAM Journal on Scientific Computing, **37**, 2, A1111-A1138 (2015).

[13] M. Bergounioux and M. Haddou, *A new relaxation method for a discrete image restoration problem*, Journal of Convex Analysis, **17**, 3, 861–883 (2010).

[14] M. Bergounioux and A. Srour, *A relaxation approach for smooth tomographic reconstruction of binary axially symmetric objects*, Pacific Journal of Optimization, **5**, 1, 39-51 (2009).

[15] M. Bergounioux and E. Trélat, *A variational method using fractional Sobolev spaces for tomographic reconstruction of blurred and noised binary images*, Journal of Functional Analysis, **259**, 2296–2332 (2010).

[16] M. Bergounioux, E. Le Pennec and E. Trélat, *Fractional-order variational numerical methods for tomographic reconstruction of binary images*, preprint, https://hal.archives-ouvertes.fr/hal-01794224v1

[17] J.P. Bruandet, F. Peyrin, J.M. Dinten and M. Barlaud, *3D tomographic reconstruction of binary images from cone-beam projections: a fast level-set approach*, IEEE International Symposium on Biomedical Imaging, 677- 680 (2002).

[18] L. Caffarelli and L. Silvestre, *An extension problem related to the fractional Laplacian,* Comm. Partial Differential Equations **32** (7–9), 1245–1260 (2007).

[19] G. Carlier,and I. Ekeland, *Matching for teams*, Econ. Theory, **42**, 2, 397-418 (2010).

[20] E. Casas, K. Kunisch and C. Pola, *Regularization by Functions of Bounded Variation and Applications to Image Enhancement*, Applied Mathematics and Optimization **40**, 229-257 (1999).

[21] A. Chambolle, *An algorithm for total variation minimization and applications*, Journal of Mathematical Imaging and Vision **20**, 1-2 89-97 (2004).

[22] J.-M. Dinten, *Tomographie à partir d'un nombre limité de projections : régularisation par champs markovien*, PHD thesis, Université Paris-Sud (1990).

[23] N.J. Dusaussoy, *Image reconstruction from projections*, SPIE's international symposium on optics, imaging and instrumentation, San Diego (1994).

[24] D. Gottlieb and C.-W. Shu, *On the Gibbs phenomenon and its resolution*, SIAM Rev. **39**, 4, 644- 668 (1997).

[25] M. Greenblatt, *A method for proving L^p boundedness of singular Radon transforms in codimension one for* $1 < p < \infty$, Duke Math. J. **108**, 2, 363- 393 (2001).

[26] S. Helgason, *The Radon Transform*, Birkhäuser, Basel (1980).

[27] S. Helgason, *Ranges of Radon transforms*, Computed tomography (Cincinnati, Ohio, 1982), Proc. Sympos. Appl. Math., **27**, 63-70, Amer. Math. Soc., Providence, R.I (1982).

[28] A. Hertle, *On the range of the Radon transform and its dual*, Math. Ann. **267**, 1, 91-99 (1984).

[29] K. Hanson, *Tomographic reconstruction of axially symmetric objects from a single radiograph*, High Speed Photography, **491** (1984).

[30] G. Herman, *Image reconstruction from projections: the fundamentals of computerized tomography*, Academic Press (1980).

[31] B .Hofmann, B. Kaltenbacher, C. Pöschl and O. Scherzer, *A convergence rates result for Tikhonov regularization in Banach spaces with non-smooth operators*, Inverse Problems **23**, 987–1010 (2007).

[32] A.C. Kak and M. Slaney, *Principles of Computerized Tomographic Imaging*, New York, IEEE Press (1988).

[33] S. Krimme, J. Baumann, Z. Kiss, A. Kuba, A. Nagy and J. Stephan, *Discrete tomography for reconstruction from limited view angles in non-destructive testing*, Electronic Notes in Discrete Mathematics, Proceedings of the Workshop on Discrete Tomography and its Applications, **20**, 455-474 (2005).

[34] M. Magnor, G. Kindlmann, C. Hansen and N. Duric, *Reconstruction and visualization of planetary nebulae*, IEEE Trans. Visualization Computer Graphics **11**, 5 , 485-496 (2005).

[35] R. Neelamani, H. Choi, and R. Baraniuk, *ForWaRD: Fourier-wavelet regularized deconvolution for ill-conditioned systems*, IEEE Trans. Signal Process., **52**, 2, 418-433 (2004).

[36] F. Natterer, *Exploiting the ranges of Radon transforms in tomography*, Numerical treatment of inverse problems in differential and integral equations, Progr. Sci. Comput., 2, Birkhäuser, Boston, Mass., 290-303 (198).

[37] P. Petrushev and Y. Xu, *Localized polynomial frames on the interval with Jacobi weights*, J. Fourier Anal. Appl. **11**, 5, 557-575 (2005).

[38] J.A. Sethian, *Theory, algorithms and applications of level set methods for propagating interfaces*, Acta Numerica, **5**, 309-395, (1996).

Maïtine Bergounioux
Institut Denis Poisson - UMR 7013
Université d'Orléans
BP 6759 F-45067 Orléans Cedex 2
France
e-mail: maitine.bergounioux@univ-orleans.fr

Isabelle Abraham
CEA Ile de France- BP 12, 91680 Bruyères le Châtel, France
e-mail: Isabelle.Abraham@cea.fr

Romain Abraham
Institut Denis Poisson - UMR 7013
Université d'Orléans
BP 6759 F-45067 Orléans Cedex 2
France
e-mail: romain.abraham@univ-orleans.fr

Guillaume Carlier
CEREMADE, UMR CNRS 7534, Université Paris IX Dauphine, Pl. de Lattre de Tassigny, 75775 Paris Cedex 16, France
e-mail: carlier@ceremade.dauphine.fr

Erwan Le Pennec
CMAP, École polytechnique, CNRS, Université Paris-Saclay, 91128, Palaiseau, France.
e-mail: erwan.le-pennec@polytechnique.edu

Emmanuel Trélat
Sorbonne Université (Paris 6) Laboratoire Jacques-Louis Lions, CNRS Inria, équipe CAGE 4 place Jussieu, BC 187 75252 Paris cedex 05, France
e-mail: emmanuel.trelat@sorbonne-universite.fr